Geological Society of America
Special Paper 409
2006

Cumulate xenoliths in Oligocene alkaline basaltic and lamprophyric dikes from the eastern Rhodopes, Bulgaria: Evidence for the existence of layered plutons under the metamorphic core complexes

Peter Marchev*
Geological Institute, Bulgarian Academy of Sciences,
Acad. G. Bonchev St., 1113 Sofia, Bulgaria
Shoji Arai
Department of Earth Sciences, Kanazawa University,
Kakuma, Kanazawa 920-1192, Japan
Orlando Vaselli
Dipartimento di Scienza della Terra, Via G. La Pira, 4, 50121 Firenze, Italy

ABSTRACT

Ultramafic and mafic xenoliths entrained in late Oligocene dikes of intraplate origin provide information about the composition of the lower crust and the processes operating beneath the eastern Rhodope metamorphic core complexes Biala Reka and Kesebir, in southeastern Bulgaria. The cumulates comprise a series of high- to medium-pressure rocks represented by olivine websterites, orthopyroxenites, clinopyroxenites, websterites, and gabbros. Thermobarometric studies and comparison with experimental works suggest that the cumulate sequence formed from hydrous (>3 wt%) mafic magma at pressures of 14–9 kilobars (45–30 km) and temperatures of 1200–850 °C.

It is inferred that underplating of such hot, wet mafic intrusions modified the thermal and mechanical properties of the lower and middle crust, as is reflected in thermal metamorphism, associated extension, and hydrothermal activity producing low-sulfidation Au deposits. Findings of similar xenoliths in the alkaline basalts from other extended regions such as the eastern Mediterranean and the Basin and Range Province indicate that underplating of mafic magma plays an important role in core complex formation.

Keywords: eastern Rhodopes, metamorphic core complex, underplating, ultramafic and mafic xenoliths

*E-mail: pmarchev@geology.bas.bg.

Marchev, P., Arai, S., and Vaselli, O., 2006, Cumulate xenoliths in Oligocene alkaline basaltic and lamprophyric dikes from the eastern Rhodopes, Bulgaria: Evidence for the existence of layered plutons under the metamorphic core complexes, *in* Dilek, Y., and Pavlides, S., eds., Postcollisional tectonics and magmatism in the Mediterranean region and Asia: Geological Society of America Special Paper 409, p. 237–258, doi: 10.1130/2006.2409(13).

INTRODUCTION

Intrusion of mantle-derived magmas at or near the base of the crust, known also as mantle underplating, is believed to be the major process causing extension in the tectonic areas where metamorphic core complexes are developed (Gans, 1987; Gans et al., 1989; Wilshire, 1990; Fyfe, 1992; White, 1992). The consequences of underplating of mafic magma are twofold: (1) it may significantly modify the thermal and mechanical properties of the crust, thus enhancing deformation and strain localization in an extensional environment (Lynch and Morgan, 1987; Chèry et al., 1989; Gans et al., 1989; Geoffroy, 1998; Corti et al., 2003), and (2) it causes the production of more evolved magmas either by fractional crystallization and crustal contamination or by partial melting, which in turn transfers heat from the lower crust into the middle crust (Hill et al., 1995).

The role of differentiated granite-granodiorite intrusions in the formation of local topographic culminations has been clarified by many authors (Lister and Baldwin, 1993; Hill et al., 1995; MacCready et al., 1997). These authors argue that granite-granodiorite intrusions, transferring the heat from lower to middle crust, heat the crust above the normal geothermal gradient and facilitate deformation and mylonite formation. Although it is widely accepted that underplating plays a major role in core complex formation, examples of mantle-derived magmas and studies of their effect on the formation of the core complexes are still missing. The major problem in clarifying these issues is the lack of access to the deepest levels of the core complex structures. Numerous xenolith suites (e.g., Conrad and Kay, 1984; Ho et al., 2000; Sachs and Hansteen, 2000; Dobosi et al., 2003; Cvetković et al., 2004; Kovács et al., 2004) as well as large masses of tectonically exposed igneous pyroxenites and gabbros from the mantle-crust transition in oceanic (e.g., Kohistan, Pakistan, and the Talkeetna area, Alaska; Coward et al., 1986; DeBari and Coleman, 1989) and continental (e.g., the Ivrea zone and Val Malenco in the Alps; Rivalenti et al., 1981; Hermann et al., 2001) arc settings have been reported, but none of them has been related to core complex formation. Descriptions of xenoliths from metamorphic core complex–associated magmatism come from two areas: the Menderes massif in Turkey (Çakir et al., 1999) and the core complex belt in southeastern California and western Arizona (Wilshire, 1990), both of which exhibit many evolutionary similarities to the southeast Bulgarian metamorphic core complexes discussed here (see Marchev et al., 2004b). Petrological studies by Rivalenti et al. (1984) and structural studies by Quick et al. (1994) suggest that mafic underplating in the Ivrea zone occurred in an extensional setting. Thus, the Ivrea zone seems to be another suitable candidate for the processes that might occur in the deepest levels of a core complex.

Studies of the xenoliths entrained in the late Krumovgrad alkaline basaltic dikes in the eastern Rhodopes provide an unusually deep view into the mantle and the lower crust of two metamorphic core complexes and an opportunity to test the models proposed for the role of the magmatism in the core complex formation. Here we provide preliminary data on the mineral composition and texture of these xenoliths and calculate the *P-T* conditions of their crystallization. On the basis of these data, we conclude that ultramafic and mafic magmas crystallized at depths of 40–30 km, close to or beneath the current Moho. We speculate that this magmatism may have provided the heat and fluids for thermal and hydrothermal events during the late Eocene (38–35 Ma).

GEOLOGICAL FRAMEWORK

Geological Setting

The eastern Rhodopes occupy the eastern part of the Rhodope metamorphic province. The latter is a large accretionary orogen that is regarded as the most internal zone of the Alpine-Himalayan orogenic system in the eastern Mediterranean region, outcropping mainly in southern Bulgaria and northern Greece (Fig. 1). The Rhodope massif is bounded to the north against the Srednogorie zone by the Maritsa fault. To the west, it is separated from the Serbo-Macedonian massif by a tectonic contact interpreted as a Middle Miocene–Late Pliocene detachment fault (Dinter and Royden, 1993). The southern and southeastern parts of the massif are hidden beneath the Aegean Sea and the Thrace basin.

According to recent ideas, the Rhodope massif is a complicated Alpine nappe structure (e.g., Ivanov, 1989; Burg et al., 1990, 1996) that consists of amphibolite-facies metamorphic basement derived from magmatic and sedimentary protoliths locally enclosing eclogites. The pre-Alpine history of the massif is poorly known. Available data suggest the existence of extensive Late Carboniferous magmatism (290–310 Ma; Liati and Gebauer, 1999; Ovtcharova et al., 2002; Peytcheva et al., 2004; Ovtcharova, 2005) and accompanying metamorphism (Carrigan et al., 2003). Magmatism of Late Neoproterozoic age (572 ± 5 Ma) and much older ages (3230–1600 and 2500–660 Ma) from a few inherited zircon cores (Liati and Gebauer, 2001; Carrigan et al., 2003) suggests that the metamorphic basement is Variscan or older.

In Alpine times, the Rhodope Massif was characterized by a complicated tectono-metamorphic evolution. Ivanov (1989) and Burg et al. (1990) recognized two major phases or deformation styles within the evolution of the massif. The first compressional stage, with large-scale south-vergent thrusting and amphibolite-facies metamorphism, was suggested to have culminated during the Middle Cretaceous (110–90 Ma; Zagortchev and Moorbath, 1986). The subsequent extensional phase involved exhumation of the thrust complex, formation of a brittle-ductile detachment, and core complex development. It was proposed to have been initiated in the Late Cretaceous by the emplacement of weakly deformed granitoid bodies dated at ca. 80 Ma (Peytcheva et al., 1998), and then to have been continued with the formation of Early Tertiary graben structures filled with continental sediments and volcanic rocks.

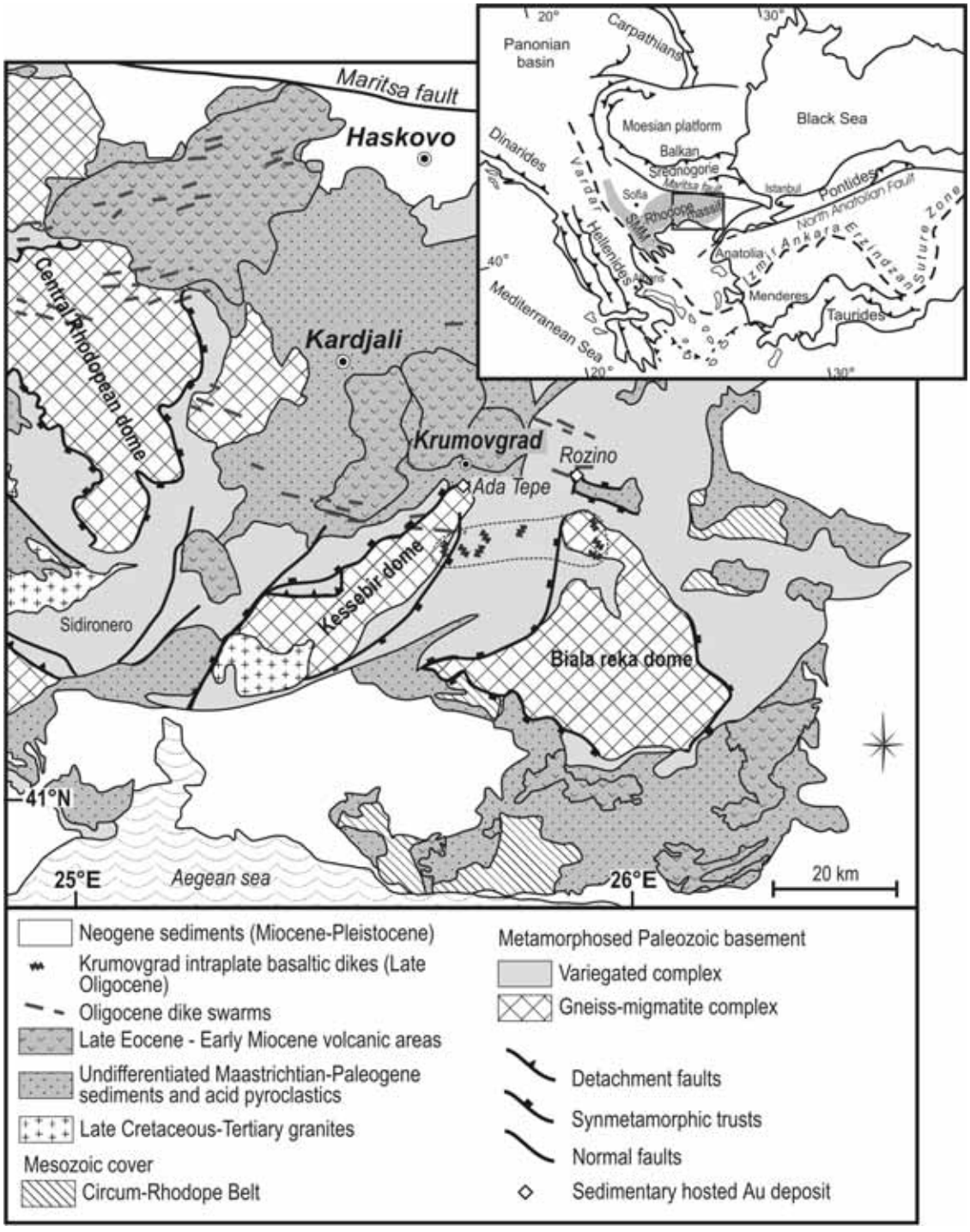

Figure 1. Schematic geologic map of the eastern Rhodopes compiled from Ricou et al. (1998), Yanev et al. (1998), Marchev et al. (1998a,b), and Bonev et al. (2005). Outlined is the distribution of the alkaline basaltic dikes. The inset shows the position of the Rhodope massif with respect to the major tectonic units in southeastern Europe. SMM—Serbo-Macedonian massif.

Regional Geology of the Eastern Rhodope Region

Metamorphic rocks in the eastern Rhodope region in Bulgaria and Greece consist of tectonometamorphic complexes that are characterized by different degrees of metamorphism and geochronologic ages (Mposkos and Krohe, 2000). These units are separated, at least locally, by tectonic contacts of predominantly extensional origin (Krohe and Mposkos, 2002). In Bulgaria, they are represented by a gneiss migmatite complex as the lowermost structural unit and an overlying variegated complex of mixed metasedimentary and metaigneous protoliths as an upper structural unit (Kozhoukharov et al., 1988; Haydoutov et al., 2001). These metamorphic complexes represent the lower- and upper-plate rocks of the extensional low-angle detachment fault systems. The upper tectonic unit comprises interlayered amphibolites, marbles, various schists, and gneisses enclosing eclogite lenses and metaophiolites. The lower tectonic unit is composed of para- and predominant orthogneisses and migmatitic gneisses, intercalated at different stratigraphic levels with schists and amphibolites.

Core complex development in the eastern Rhodopes was part of the protracted extensional history of the Rhodope massif. Local evidence indicates that crustal extension may have begun as early as the Late Cretaceous. It is marked by metamorphism in the upper (variegated) complex (73–62 Ma; Liati et al., 2002) and emplacement of a series of granitoids at the Biala reka dome (ca. 70 Ma; Marchev et al., 2004b) and by undeformed metamorphic pegmatites (65 Ma; Mposkos and Wawrzenitz, 1995). This suggests that both midcrustal granite intrusion and mantle to lower-crustal metamorphism occurred at the same time, marking the initiation of the extensional development of the core complex.

Extension along continuously mappable low-angle detachment faults formed the Biala Reka and Kessebir metamorphic core complexes (Burg et al., 1996; Ivanov et al., 2000; Mposkos and Krohe, 2000; Bonev, 2002; Krohe and Mposkos, 2002) and led to the formation of sedimentary basins with several unconformities developed during syntectonic continental and marine sedimentation and exhumation of ultra-high-pressure metamorphic lithologies. Continental clastic sedimentation started in Maastrichtian–Palaeocene time in the area north of the Kessebir dome structure (Goranov and Atanasov, 1992; Boyanov and Goranov, 1994, 2001), which is coeval with or slightly younger than Late Cretaceous metamorphism and granitoid magmatism. Metamorphism, uplift, and cooling of the Variegated Complex from 500 °C to 300–350 °C was suggested to have occurred in the age interval 45–39 Ma (Bonev et al., 2005) on the basis of the $^{40}Ar/^{39}Ar$ ages from amphibole and muscovite determined by Mukasa et al. (2003). Similar timing of the metamorphism, exhumation, and cooling (47–35 Ma) was suggested for the analogous unit of the eastern part of the central Rhodope dome by U-Pb and $^{40}Ar/^{39}Ar$ dating of monazite and biotite, respectively (Ovtcharova, 2005). Cooling and exhumation of the lower unit from the Kessebir dome occurred between 38 and 37 Ma (Bonev et al., 2005), followed by normal faulting under brittle conditions, accompanied by hydrothermal activity and formation of the high-grade low-sulfidation Au deposits Ada Tepe and Rosino at 35–36.5 Ma (Fig. 1; Marchev et al., 2003, 2004a; Bonev et al., 2005). Similar cooling or exhumation ages of between 42 and 36 Ma for the lower unit have been obtained for the Greek part of the two structures based on K-Ar ages by Lips et al. (2000) and Krohe and Mposkos (2002) and for the central Rhodope dome (37–35 Ma) on the basis of U-Pb dating of monazite and $^{40}Ar/^{39}Ar$ dating of biotite by Ovtcharova (2005).

Widespread late Eocene–Oligocene volcanism (39–26 Ma), developed in several volcanic areas coeval or subsequent to sedimentary basin formation, is an important feature of the geology of the eastern Rhodope. It is dominated by intermediate to acid lavas and associated volcaniclastic products and by subordinate basic varieties (Harkovska et al., 1989; Marchev et al., 1998a). The temporal and spatial coincidence of these events with the late-stage episode of extension suggests that the volcanism was synextensional (Marchev et al., 2004b) rather then collision-related (Yanev and Bardintzeff, 1997; Yanev et al., 1998). Magmatic activity in the two dome structures terminated with the emplacement of numerous xenolith-bearing dikes of intraplate basalt (the Krumovgrad alkaline basalts; Marchev et al., 1997, 1998b), which are the subject of the current article.

Krumovgrad Alkaline Basalts

Xenolith-bearing alkaline basaltic dikes (Mavroudchiev, 1964; Marchev et al., 1997, 1998b, 2004b) are located 20–30 km southeast of the town of Krumovgrad (Fig. 1). The emplacement of the dikes is controlled by three major fault systems, striking east-west, north-south, and northwest-southeast. The dikes crop out over an east-west-oriented area of 1000 km^2 in the Biala Reka and Kessebir domes. They were intruded into both the gneiss-migmatite and the variegated complexes of the Rhodopean metamorphic basement at ca. 26–28 Ma (Marchev et al., 1997). Most of the dikes are 0.5–2 m thick, except a north-south-striking dike that is up to 40 m thick.

The dikes have basanitic to lamprophyric (camptonite) compositions (Marchev et al., 1998b). Olivine and clinopyroxene are the most common phenocrysts in the basanites from the western dikes, accompanied by amphibole megacrysts in the lamprophyres from the eastern dikes. Sanidine and biotite are rare. The groundmass in the basanites is fine-grained in the small dikes and near contacts of thicker dikes. The groundmass is holocrystalline in the interior of the largest dike, which is composed of microlites of Ti-augite, plagioclase, amphibole, Fe-Ti-oxides, and interstitial K-feldspar, analcite, and biotite. The panidiomorphic groundmass is typical of the lamprophyres. It contains euhedral kaersutite and plagioclase, as well as lesser clinopyroxene and magnetite grains with abundant interstitial analcite and sanidine.

The Krumovgrad alkaline basalts have high $^{143}Nd/^{144}Nd$ (0.51290–0.51289), low $^{87}Sr/^{86}Sr$ (0.70323–0.70338), and high

$^{206}Pb/^{204}Pb$ (19.02–18.91) at relatively low $^{207}Pb/^{204}Pb$ ratios (15.64–15.52), which is interpreted to indicate a source similar to that of the European asthenospheric reservoir defined by Wilson and Downes (1991).

Xenolith Sampling and Analytical Methods

Xenoliths were observed in three dikes; however, more than 90% of the studied samples were collected from the largest dike in the area. From about thirty samples collected, eighteen were chosen for detailed mineralogical and geochemical studies, but only two were large enough for bulk chemical analysis.

The modal mineralogy and crystallization sequence of the Krumovgrad xenoliths are presented in Table 1. Minerals were analyzed for major elements on an automatic wavelength-dispersive JEOL Superprobe 8800R at Kanazawa University and on a JEOL 870 Superprobe at the University of Florence using the ZAF and Bence and Albee (1968) correction methods, respectively. Typical operating conditions were 20 keV accelerating potential, 20 nA beam current, and 3μm beam diameter at Kanazawa and 15 keV accelerating potential, 20 nA beam current, and 1 μm beam diameter at Florence. Natural and synthetic minerals were used for standards. Most reported analyses represent the average of at least two single-point analyses.

The whole-rock compositions of the two large xenoliths were determined using a Rigaku 3270 X-ray spectrometer on fused pallets at the Department of Earth Science, University of Kanazawa. In order to avoid contamination by the host basalts, the outermost zone of the xenoliths was removed by cutting with a diamond-disk saw. The xenoliths were crushed by hand in steel mortars and ground in an agate swingmill. The XRF analyses were performed under an accelerating voltage of 50 kV and a beam current of 20 mA.

Age of the Cumulates

Dating of the xenoliths entrained in high-temperature host lavas is problematic, because all of them were heated above the blocking temperature of most geothermometers (600–700 °C). In situ U-Pb dating of zircon crystals observed in some thin sections might be suitable and has been planned in the near future.

The age of the host basalts constrains the age of the xenoliths to 26–28 Ma. However, the findings from salitic xenocrysts, similar to those from some xenolithic lithologies in the 32–31 Ma lavas of the neighboring volcanic rocks (Raicheva, 2004, personal commun.), suggest that the cumulates might be older than 31 Ma.

Xenolith Rock Types, Texture, and Structure

Xenoliths in the Krumovgrad alkaline basalts are of three dominant types: (1) mantle peridotites, (2) ultramafic and mafic cumulates, and (3) metamorphic rocks from the Rhodopean metamorphic basement. Mantle xenoliths and xenoliths from the metamorphic basement are beyond the scope of this article, which is focused on the igneous cumulate rocks.

Ultramafic and mafic cumulate xenoliths are rounded to subrounded, rarely rectangular, ranging in size from <1–7 cm. They are composed of variable amounts of olivine, clinopyroxene, orthopyroxene, amphibole, plagioclase, and minor sulfides, spinel, and apatite; some contain interstitial fresh or devitrified glass. The xenoliths can be divided on the basis of mineral assemblages into two groups: ultramafic and gabbroic. The ultramafic xenoliths may be further subdivided into olivine websterites, websterites, clinopyroxenites, and orthopyroxenites. The gabbroic group is divided on the basis of the pyroxene composition into two-pyroxene gabbro and clinopyroxene gabbro.

TABLE 1. MODAL CHARACTERISTICS OF REPRESENTATIVE XENOLITHS

Rock type (Mineral phases in order of abundance)	Samples and comments
(1) Olivine websterites	
(Ol = Cpx > Opx >> Sulf)	Bz24-3 (Fig. 3A)
(2) Clinopyroxenites	
(Cpx >>Amph)	IIEG7
(Cpx = Amph >> Sp = Sulf)	Bz24-5a; amphibole clinopyroxenite (Fig. 3E)
(Cpx >> Sulf = Ap)	Bz24; high-Na-Fe salite
(Cpx > Sulf > Ilm > Ap)	Eg97-4a; ore clinopyroxenite (Fig. 4B)
(3) Websterites	
(Cpx > Opx >> Amph)	Eg97-1; two generations of clinopyroxene (Fig. 3B)
(Cpx > Opx)	IIEG99-2; two generations of clinopyroxene
(4) Orthopyroxenites	
(Opx >> Cpx)	Bz24-1
(Opx >> Ol)	IIEG14
(5) Two-pyroxene gabbro	
(Pl > Opx = Cpx >> Sulf)	Bz24-5b (Figs. 2C, 3F)
(6) Clinopyroxene gabbro	
(Cpx > Pl >> Sulf = Ilm)	Bz03-2/5 (Fig. 2B)
(Cpx, Pl, pyrite)	Bz24-5c; augite gabbro

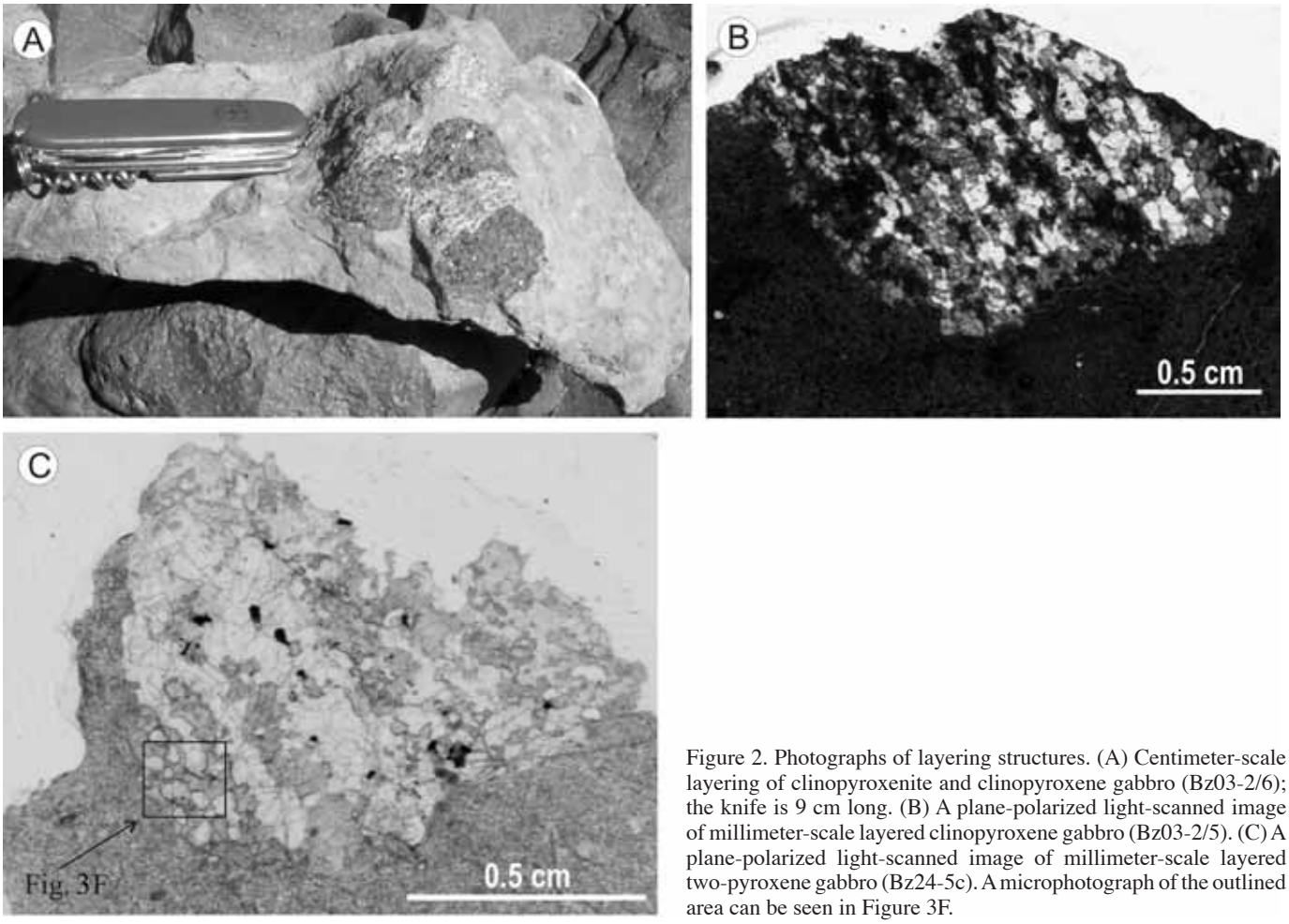

Figure 2. Photographs of layering structures. (A) Centimeter-scale layering of clinopyroxenite and clinopyroxene gabbro (Bz03-2/6); the knife is 9 cm long. (B) A plane-polarized light-scanned image of millimeter-scale layered clinopyroxene gabbro (Bz03-2/5). (C) A plane-polarized light-scanned image of millimeter-scale layered two-pyroxene gabbro (Bz24-5c). A microphotograph of the outlined area can be seen in Figure 3F.

Modal layering was observed in some clinopyroxenite-gabbro and two-pyroxene gabbro xenoliths (Fig. 2). It is defined by alternation of centimeter-scale clinopyroxenite and clinopyroxene gabbro in sample Bz03-2/6 (Fig. 2A) or millimeter-scale alternation of plagioclase and clinopyroxene in the clinopyroxene gabbro in sample Bz03-2/5 (Fig. 2B) or of plagioclase, orthopyroxene, and clinopyroxene in the two-pyroxene gabbro in sample Bz24-5c (Fig. 2C).

Olivine Websterites. These rocks are represented only by sample Bz24-3. It is dominated by large (up to 5.0 mm) olivine grains with well-expressed kink banding (Fig. 3A), clinopyroxene, and rare orthopyroxene. Blobs of sulfides are common.

Websterites. These rocks are medium- to coarse-grained with cumulitic texture. They are composed mostly of orthopyroxene and clinopyroxene with minor amphibole in sample Eg97-1 (Fig. 3B). The corroded and rounded amphibole crystals in this sample appear to have crystallized before the host clinopyroxene. At the junction of orthopyroxene and clinopyroxene crystals, websterites contain pockets of light to dark brown glass and/or crypto- to microcrystalline aggregates.

Clinopyroxenites. These rocks are medium- to coarse-grained with clinopyroxene crystals up to 5.0 mm in length. Four different types of clinopyroxenites can be distinguished on the basis of clinopyroxene composition and associated minerals: augite clinopyroxenites (IIEG7, IIEG18, Bz24-3c); salite clinopyroxenites (Bz24, Bz03-2/6); ore (ilmenite-sulfide) clinopyroxenites (Eg97-4a); and hornblende-pyroxenites (Bz24-5a, 26-2a). Ilmenite and magnetite (Fig. 3C), ilmenite and sulphide blebs (Fig. 4A), spinel, and apatite are present mainly in the salite clinopyroxenites. A distinctive ore clinopyroxenite, sample Eg97-4a, contains subhedral cumulus grains of apatite and clinopyroxene surrounded by intercumulus sulfides and ilmenite (Fig. 4B). These textural and mineralogical features suggest an origin by emplacement of volatile- and sulfide-rich melt. The presence of a large quantity of apatite and Ni and Co-enriched sulfide minerals suggest that P and S played a major role in the separation of the iron-oxide-sulfide melt and was an important constituent of the volatile phase. Amphibole is present in trace in sample IIEG7 (Fig. 3D) up to ~50% in the amphibole clinopyroxenites (Bz24-5; Fig. 3E), with textural

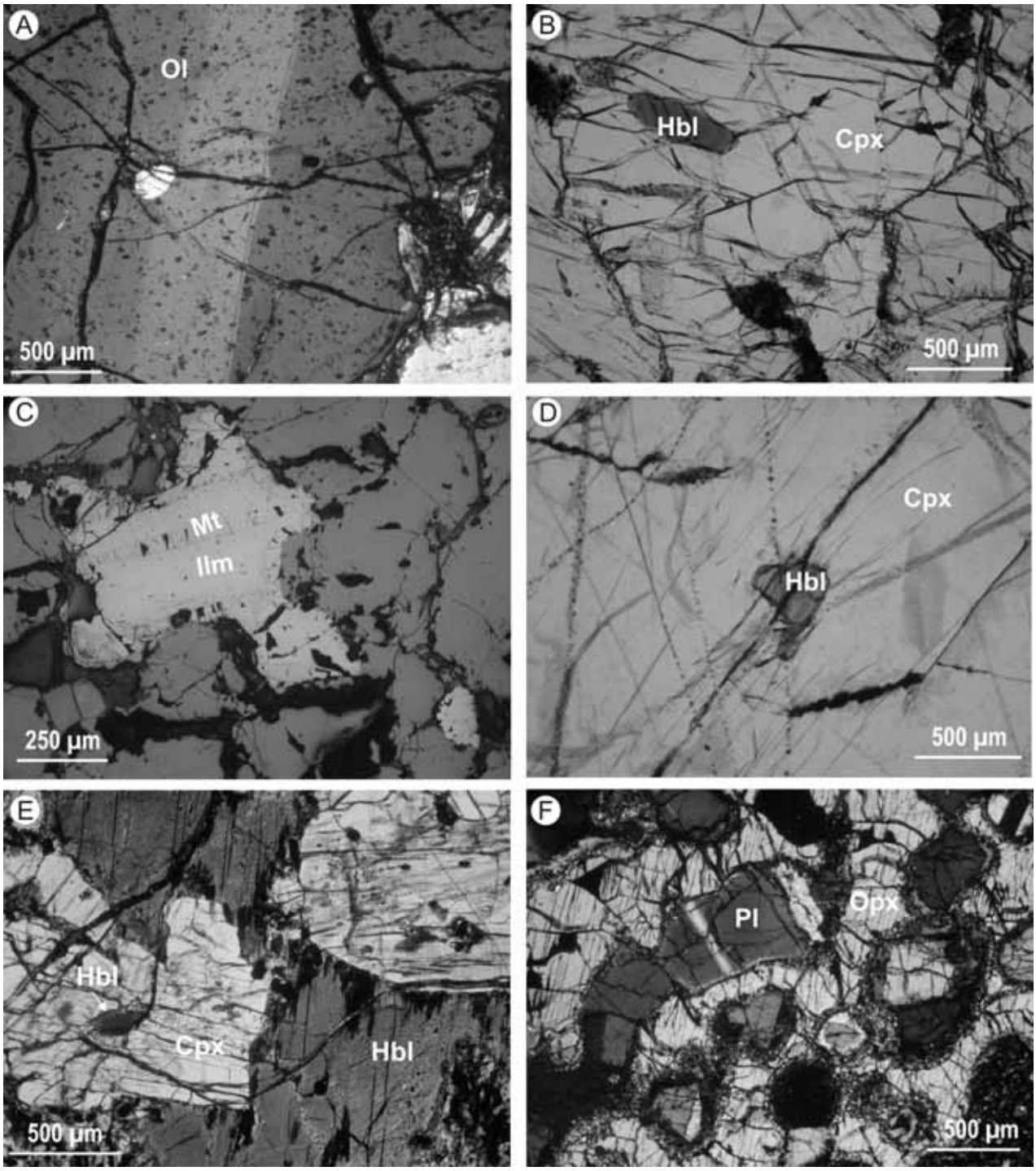

Figure 3. Photomicrographs of the Krumovgrad xenoliths. (A) Olivine (Ol) websterite. The olivine shows kink banding. (B) Corroded and rounded hornblende crystals (Hbl) included in clinopyroxene (Cpx); websterite Eg97-1. (C) Ilmenite-magnetite (Ilm-Mt) intergrown in high-Fe salite clinopyroxenite (Bz03-2/6). Ti-magnetite forms elongated crystals. (D) Clinopyroxenite with textural relationships showing that amphibole replaces clinopyroxene grains; sample IIEG7. (E) Hornblende-clinopyroxenites (Bz24-5a). The hornblende poikilitically encloses clinopyroxene and small amphibole blebs within the clinopyroxene, showing that amphibole is replacing clinopyroxene. (F) Zoned subhedral to rounded crystals of plagioclase (Pl) included in intercumulus high-Fe orthopyroxene. The orthopyroxene crystals show thin reaction rims of clinopyroxene with the plagioclase; sample from two-pyroxene gabbro Bz25-5b.

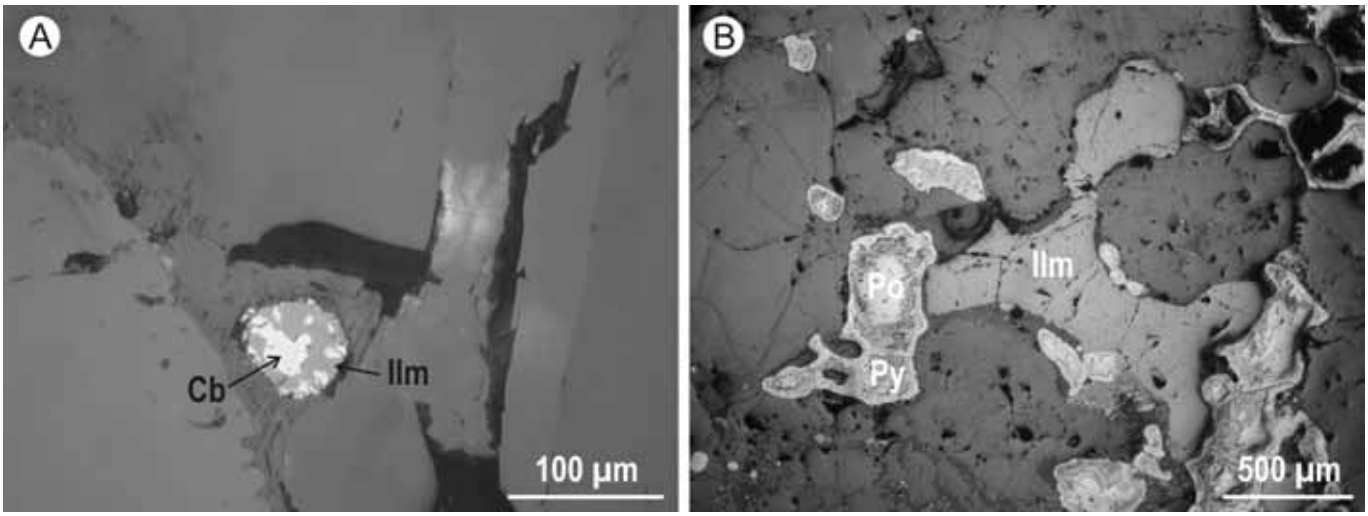

Figure 4. Sulfides in the Krumovgrad cumulates: (A) A cubanite-ilmenite (Cb-Ilm) globule in plagioclase close to the boundary with green clinopyroxene in clinopyroxenite Bz03-2/5. (B) Intercumulus sulfides (pyrrhotite-cubanite) and ilmenite in ore clinopyroxenite (Py) Eg97-4a.

relationships showing that amphibole replaces or poikilitically encloses clinopyroxene grains. This is evidenced by ragged clinopyroxene crystals and abundant patches of the amphibole within the clinopyroxene crystals.

Orthopyroxenites. This group is represented by two samples ~2 cm in diameter. They are almost entirely composed of coarse orthopyroxene crystals with traces of clinopyroxene (Bz24-1) and olivine (IIEG14). Rare spinel inclusions were observed in Bz24-1.

Clinopyroxene Gabbro. These xenoliths are feldspar-rich rocks with plagioclase constituting more than 50% of the rock. They can be divided into salite gabbro (Bz03-2/5, Bz03-2/6) and augite gabbro (Bz24-5c). The former are among the most abundant and largest xenoliths, reaching up to 7 cm. They show typical cumulate texture consisting of cumulus plagioclase and intercumulus green (salitic) clinopyroxene accompanied by rare early apatite and sulfides. The sieve textures in the clinopyroxene suggest incipient partial melting. The augite gabbro (Bz24-5c) is coarser-grained than the salite gabbro. The textural relationships suggest simultaneous crystallization of the clinopyroxene and plagioclase. Early cubanite is found in the clinopyroxene.

Two-Pyroxene Gabbro. This gabbro (Bz24-5b) shows well-expressed layering with aligned subhedral clusters of enstatite or clinopyroxene enclosing euhedral plagioclase crystals. Orthopyroxene shows thin reaction rims of clinopyroxene with the plagioclase (Fig. 3F).

Whole-Rock Chemistry of Websterites and Gabbro

The whole-rock major- and trace-element compositions for a websterite and a gabbro are shown in Table 2.

TABLE 2. MAJOR-ELEMENT COMPOSITION OF TWO CUMULATE SAMPLES

Rock type	Websterite	Gabbro
Sample N	IIEg99-2	Bz03-2/5
SiO_2	49.61	52.05
TiO_2	0.29	0.35
Al_2O_3	4.86	16.40
FeOt	9.43	5.10
MnO	0.19	0.10
MgO	16.87	9.69
CaO	15.47	15.15
Na_2O	0.89	2.40
K_2O	0.49	0.69
P_2O_5	0.04	0.04
Total	98.14	101.97

The major-element abundance patterns are in accordance with the cumulus mineralogy. Websterite IIEG99-2 has high MgO (16.8 wt%) and CaO concentrations, whereas gabbro Bz03-2/5 is depleted in MgO (9.7 wt%) and enriched in CaO and Al_2O_3. Both samples are silica-undersaturated with low contents of TiO_2, K_2O, and P_2O_5.

Mineral Chemistry

Olivine. Olivine was found only in the olivine websterite Bz24-3 and orthopyroxenite IIEG14 from the ultramafic cumulate sequence. Representative analyses are given in Table 3. The forsterite content of the olivine is similar (around 83–84) in the two samples. The CaO contents vary between 0.03 and

TABLE 3. REPRESENTATIVE MICROPROBE ANALYSES OF OLIVINE AND ORTHOPYROXENE IN THE KRUMOVGRAD XENOLITHS

Mineral	Ol	Ol	Opx	Opx	Opx	Opx	Opx
Rock type	Ol webst	Opxite	Opxite	Opxite	Webst	Webst	2-px gabbro
Sample no.	Bz 24-3	IIEG14	IIEG14	Bz24-1	IIEG99-2	EG97-1	Bz24-5b
SiO_2	40.40	40.04	55.17	56.96	54.15	54.23	52.07
TiO_2	0.01	0.01	0.21	0.05	0.05	0.03	0.19
Al_2O_3	0.00	0.01	2.74	1.41	3.37	3.02	1.60
Cr_2O_3	0.01	0.00	0.12	0.20	0.14	0.16	0.05
FeO	15.45	16.30	10.36	7.58	14.43	14.92	26.36
MnO	0.24	0.23	0.20	0.15	0.29	0.34	0.74
MgO	46.31	44.83	30.73	33.61	27.67	28.01	18.48
CaO	0.08	0.08	1.03	0.86	0.91	0.91	1.33
Na_2O			0.04	0.04	0.03	0.05	0.04
K_2O			0.01	0.00	0.01	0.02	0.01
NiO	0.18	0.39	0.10	0.11	0.00	0.03	0.01
Total	102.70	101.89	100.71	100.97	101.05	101.72	100.88
Mg #	84.2	83.1	84.1	88.8	77.4	77.0	55.5
Wo			2.00	1.62	1.81	1.74	2.77
En			82.13	87.18	75.59	75.24	53.33
Fs			15.87	11.20	22.60	23.02	43.90
Si	0.990	0.994	1.926	1.956	1.919	1.910	1.967
Ti	0.000	0.000	0.006	0.001	0.001	0.001	0.005
Al^{IV}			0.074	0.044	0.081	0.090	0.033
Al^{VI}			0.039	0.013	0.060	0.036	0.039
Fe^{3+}			0.023	0.025	0.017	0.052	0.000
Fe^{2+}	0.317	0.338	0.280	0.192	0.411	0.388	0.833
Mn	0.005	0.005	0.006	0.004	0.009	0.010	0.024
Mg	1.692	1.659	1.599	1.721	1.462	1.471	1.041
Ca	0.002	0.002	0.039	0.032	0.035	0.034	0.054
Na			0.003	0.003	0.002	0.003	0.003
Cr			0.003	0.005	0.004	0.004	0.001
Ni	0.004	0.008	0.003	0.003	0.000	0.001	0.000

0.08 wt%, and the MnO contents are rather uniform (0.23–0.29 wt%). The NiO ranges from 0.18 to 0.39 wt%.

Clinopyroxene. Clinopyroxene (Table 4) shows a wide compositional range (Mg #, 89.0–55.0; Al_2O_3, 2.04–10.10 wt%; and Na_2O, 0.31–1.67 wt%). Those in the ultramafic group are predominantly diopsides and augites. Variations of the Mg # (up to 10) within individual rock samples are seen in the websterites and ore clinopyroxenites. Clinopyroxene exhibits two trends of compositional variation: (1) diopside to salite in the amphibole clinopyroxenites, salitic clinopyroxenites, and gabbros and (2) diopside to augite in the ore clinopyroxenites and two-pyroxene gabbro (Fig. 5). Similar trends have been observed in the pyroxenes from Adak island xenoliths (Conrad and Kay, 1984) and in the exposed ultramafic-mafic lower-crustal section from Tonsina-Nelchina (DeBari and Coleman, 1989). The high-Fe salitic clinopyroxenes in the Krumovgrad gabbros and the clinopyroxenites form a comparatively isolated group.

Clinopyroxenes from the ultramafic orthopyroxenite Bz24-1, olivine websterite Bz24-3, some websterites and clinopyroxenites, and hornblende clinopyroxenite Bz26-2a display a trend of increasing Al with decreasing Mg # (Fig. 6). Gabbros along with some websterites and clinopyroxenites are slightly displaced from that trend. Ore clinopyroxenites and two-pyroxene gabbro exhibit the lowest Al contents and variation of the Mg # between 76 and 63, forming quite a distinct subhorizontal trend. Two trends of correlation between Al and Mg #, similar to our ultramafic and ore clinopyroxenite / two-pyroxene trends, were observed for the cumulate rocks from Tonsina-Nelchina by DeBari and Coleman (1989) and DeBari (1997). These two trends have been attributed to high- and low-pressure crystallization conditions, respectively. A third trend, subparallel to that of the ultramafic rocks, has been observed in the salite clinopyroxenites and gabbros.

Orthopyroxene. Orthopyroxene ranges from bronzite (Mg # 91) in the othopyroxenite Bz24-1 to hypersthene (Mg # 55.3) in the two-pyroxene gabbro Bz24-5b (Table 3). The Ca content is low (0.86–1.33 wt%). Orthopyroxene shows a pronounced trend of Al enrichment (Fig. 6B) from high–Mg # ortho-

TABLE 4. REPRESENTATIVE MICROPROBE ANALYSES OF CLINOPYROXENES IN THE KRUMOVGRAD XENOLITHS

Rock type	Ol webst	Webst	Webst	Webst	Webst	Opxite	Cpxite	Cpxite	Cpxite	Cpxite	Cpxite	Cpxite	Ore cpxite	Ore cpxite	Hbl cpxite	Hbl cpxite	Gabbro	Gabbro	Gabbro	2-px gabbro
Sample no.	Bz24-3	IIEG99-2		EG97-1		Bz24-1	IIEG7	IIEG18	Bz24-3c	Bz03-2/6	Bz24		EG97-4a		Bz24-5a	Bz26-2a	Bz03-2/6	Bz03-2/5	Bz24-5c	Bz24-5b
SiO_2	50.76	51.18	51.51	52.21	52.51	53.83	52.04	51.97	53.27	51.21	48.30	49.32	53.12	51.39	47.70	44.98	46.12	51.78	52.64	51.92
TiO_2	0.66	0.89	0.17	0.15	0.48	0.12	0.53	0.57	0.32	0.57	1.02	0.95	0.23	0.31	1.22	3.14	1.96	0.30	0.25	0.34
Al_2O_3	4.78	4.56	4.30	3.97	4.03	2.73	5.17	4.28	2.60	2.50	4.42	4.68	1.15	1.94	6.68	10.76	8.44	4.45	3.33	1.70
Cr_2O_3	0.25	0.40	0.30	0.28	0.24	0.39	0.17	0.35	0.67	0.04	0.00	0.01	0.06	0.12	0.02	0.00	0.05	0.08	0.02	0.07
FeO	5.12	5.10	7.28	7.14	5.36	3.68	5.87	5.43	5.00	11.96	12.04	11.84	8.82	10.52	5.49	6.37	12.22	7.18	7.73	12.62
MnO	0.21	0.11	0.18	0.18	0.14	0.12	0.14	0.16	0.16	0.50	0.53	0.60	0.41	0.61	0.15	0.14	0.41	0.21	0.36	0.43
MgO	15.60	15.39	14.43	15.15	15.66	16.97	15.30	15.77	16.30	10.95	10.31	10.10	14.64	13.49	13.33	11.36	8.58	14.28	14.06	12.17
CaO	21.18	22.05	20.43	20.61	20.66	21.83	20.66	20.74	21.43	21.45	22.61	20.77	21.24	20.22	23.30	20.98	21.13	21.37	21.00	18.91
Na_2O	0.66	0.40	0.76	0.76	0.96	0.68	0.73	0.77	0.70	1.06	0.64	1.59	0.36	0.53	0.35	0.87	1.38	0.70	0.91	0.43
K_2O	0.01	0.02	0.01	0.01	0.02	0.01	0.02	0.02	0.01	0.01	0.01		0.01	0.00	0.01	0.02	0.02	0.01	0.02	0.02
NiO	0.03	0.01	0.02	0.02	0.03	0.07	0.02	0.03	0.01	0.01			0.01		0.01	0.00	0.00	0.01	0.00	0.01
Total	99.26	100.11	99.39	100.48	100.09	100.43	100.62	100.09	100.45	100.26	99.88	99.86	100.03	99.14	98.26	98.62	100.30	100.37	100.32	98.62
Mg #	84.5	84.3	78.0	79.10	83.9	89.2	82.40	83.8	85.3	62.0	60.4	60.3	74.7	69.6	81.2	76.1	55.6	78.0	76.4	63.2
Wo	45.0	46.4	44.1	43.5	44.2	45.1	44.3	44.1	44.5	46.2	48.3	46.7	43.5	42.4	50.4	50.1	49.2	45.4	44.8	41.1
En	46.1	45.1	43.3	44.5	46.6	48.8	45.6	46.6	47.1	32.8	30.7	31.5	41.8	39.4	40.1	37.8	27.8	42.2	41.8	36.8
Fs	8.9	8.5	12.6	12.1	9.2	6.1	10.1	9.2	8.4	21.0	21.0	21.8	14.7	18.2	9.5	12.1	22.9	12.3	13.4	22.2
Si	1.866	1.874	1.906	1.907	1.913	1.945	1.891	1.896	1.936	1.925	1.829	1.855	1.973	1.937	1.787	1.688	1.736	1.899	1.936	1.989
Ti	0.018	0.025	0.005	0.004	0.013	0.003	0.014	0.016	0.009	0.016	0.029	0.027	0.006	0.009	0.034	0.089	0.055	0.008	0.007	0.010
Al^{IV}	0.134	0.126	0.094	0.093	0.087	0.055	0.109	0.104	0.064	0.075	0.171	0.145	0.027	0.063	0.213	0.312	0.264	0.101	0.064	0.011
Al^{VI}	0.073	0.071	0.094	0.078	0.086	0.062	0.113	0.080	0.048	0.036	0.026	0.062	0.023	0.023	0.082	0.164	0.111	0.092	0.080	0.066
Fe^{3+}	0.064	0.023	0.036	0.052	0.035	0.023	0.014	0.037	0.029	0.083	0.134	0.145	0.015	0.057	0.086	0.033	0.141	0.040	0.034	0.000
Fe^{2+}	0.094	0.133	0.190	0.166	0.128	0.088	0.165	0.128	0.123	0.293	0.248	0.227	0.258	0.274	0.085	0.167	0.243	0.181	0.203	0.405
Mn	0.007	0.003	0.006	0.006	0.004	0.004	0.004	0.005	0.005	0.016	0.017	0.019	0.013	0.019	0.005	0.004	0.013	0.007	0.011	0.014
Mg	0.855	0.840	0.796	0.825	0.851	0.914	0.829	0.857	0.883	0.614	0.582	0.566	0.811	0.758	0.745	0.636	0.482	0.781	0.771	0.695
Ca	0.834	0.865	0.810	0.807	0.807	0.845	0.804	0.811	0.835	0.864	0.917	0.837	0.845	0.817	0.935	0.844	0.852	0.840	0.827	0.776
Na	0.047	0.028	0.055	0.054	0.068	0.048	0.051	0.054	0.049	0.077	0.047	0.116	0.026	0.039	0.025	0.063	0.101	0.050	0.065	0.032
Cr	0.007	0.012	0.009	0.008	0.007	0.011	0.005	0.010	0.019	0.001	0.000	0.000	0.002	0.004	0.001	0.000	0.001	0.002	0.001	0.002
Ni	0.001	0.000	0.001	0.001	0.001	0.002	0.001	0.001	0.000	0.000	0.000	0.000	0.000	0.000	0.000	0.000	0.000	0.000	0.000	0.000

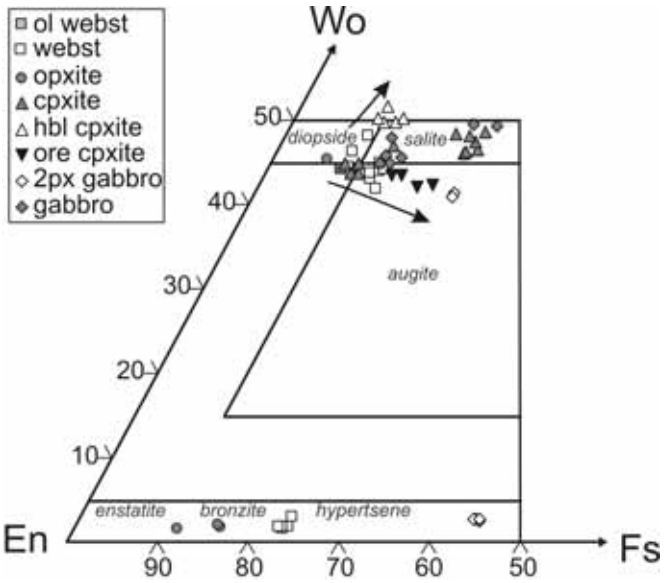

Figure 5. Pyroxene compositions of the Krumovgrad xenoliths plotted in a Wo-En-Fs triangular diagram.

pyroxenite Bz24-1 to low–Mg # websterites (Eg97-1, IIEG99-2), with two-pyroxene gabbro (Bz24-5b) falling outside of this trend.

Plagioclase. The plagioclase in the gabbro xenoliths shows overall compositional variation between An_{60} and An_{40} but smaller variation within single samples (Table 5). In the two-pyroxene gabbro, the plagioclase cores ($An_{48–40}$) are surrounded by anorthoclase rims ($An_{13}Ab_{70}Or_{17}$) (Fig. 3F). The chemical range of plagioclase in the Krumovgrad xenoliths is similar to that of gabbroic xenoliths ($An_{56–36}$) from the Pannonian basin (Kovács et al., 2004), but much lower than that from Adak island ($An_{95–88}$; Conrad and Kay, 1984).

Amphibole. The amphibole in the Krumovgrad xenoliths and megacrysts ranges from pargasite/hastingsite to kaersutite (Table 6). The variation of Mg # and TiO_2 in the xenoliths is more limited, from 71.7 to 77.8 and 0.85–3.45, respectively, with the lowest Ti, Ca, and K in the amphibole from websterite Eg97-1. These amphiboles are similar to those from the Nógrád-Gömör volcanic field, Hungary (Kovács et al., 2004), the East Eifel volcanic field (Sachs and Hansteen, 2000), and Pengu island (Ho et al., 2000). The only exception is the amphibole in hornblende clinopyroxenite Bz26-2a, which shows compositional variation and zonation similar to those in the megacrysts. These crystals are reversely zoned with an iron-rich core (Mg # 51), surrounded by a more Mg-rich rim (Mg # 77–71).

Small amphibole crystals that occur as inclusions in the clinopyroxene crystals of clinopyroxenite IIEG7 (Fig. 3D) and websterite Eg97-1 (Fig. 3B) are characterized by very high Cr content (0.32 and 0.73–0.61 wt%, respectively). However, they considerably differ in their contents of Ti and K. The concentrations of Ti and K in the amphibole from IIEG7 are similar to that of amphibole from the amphibole clinopyroxenite and megacrysts and probably have a similar origin. The strongly corroded amphibole remnants in the clinopyroxenite crystals in websterite Eg97-1 are notable for their very low Ti and K contents and minor substitution of Al^{IV} for Si. Early high-Cr amphiboles are reported in ultramafic xenoliths from olivine-augite-amphibole cumulate from Grenada (Cr up to 0.78 wt%; Arculus, 1978) and olivine clinopyroxenite from Adak island (Cr up to 0.55 wt%; Conrad and Kay, 1984). In both occurrences, it is noted that amphibole was a near-liquidus phase that crystallized before substantial clinopyroxene crystallization could deplete the melt in Cr.

Spinels and Ilmenite. Spinel is a relatively scarcely represented phase in the Krumovgrad xenoliths (Table 7). Cr-Al spinel occurs in the most Mg-rich orthopyroxenite, Bz24-1. The spinel in the amphibole clinopyroxenite Bz24-5a is Al-rich pleonaste. Fe-Ti oxides (ilmenite and magnetite) are typical of the high-Fe salitic clinopyroxenites. In these rocks, ilmenite occurs separately and is intergrown with Ti-magnetite (Bz24-5b), where it forms elongated (up to 500 μm long and 100 μm wide) crystals (Fig. 3C).

Sulfides. Most of the cumulates contain globules of sulfides. Spherical bodies of up to 70 μm are included in olivine, clinopyroxene, amphibole, and plagioclase. Intergrowth with ilmenite was also observed in the sulfide globules (Fig. 4A; Table 8). In the ore clinopyroxenites (Eg97-4a), sulfides form intercumulus crystals along with discrete ilmenite (Fig. 4B). Microprobe analyses show that the principal minerals are pyrrhotite and cubanite, with subordinate pyrite and chalcopyrite. Small amounts of Ni, Co, and Zn were detected in some sulfides.

The total of the electron microprobe analyses for most of the sulfides is between 95 and 98 wt%, with the highest and lowest values 101 and 93.5 wt%, respectively. Similar summations were obtained by Upton et al. (2000) for the sulfides from cumulates from Piton de la Fournaise, Réunion. Ion microprobe analyses by these authors confirmed that this is due to the significant amounts (>3 wt%) of oxygen in their sulfides, which might also be the case in the Krumovgrad cumulitic sulfides. Alternatively, the low total might be due to analytical error.

Estimates of Intensive Parameters for Pyroxene-Bearing Xenoliths

Temperature and Oxygen Fugacity. The temperature of crystallization of the xenoliths was estimated using the two-pyroxene geothermometers of Wood and Banno (1973) and Wells (1977), the QUILF 4.1 software of Andersen et al. (1993), and the olivine-clinopyroxene geothermometer of Loucks (1996). The QUILF program was also used to calculate the two-oxide temperatures and oxygen fugacity (fO_2) for sample Bz03-2/6. The results of the thermometric calculations are listed in Table 9. The pyroxene pairs, regarded as reflecting equilibrium at the time of crystallization, indicate temperatures of 1070–900 °C, decreasing from olivine websterite toward gabbro. The

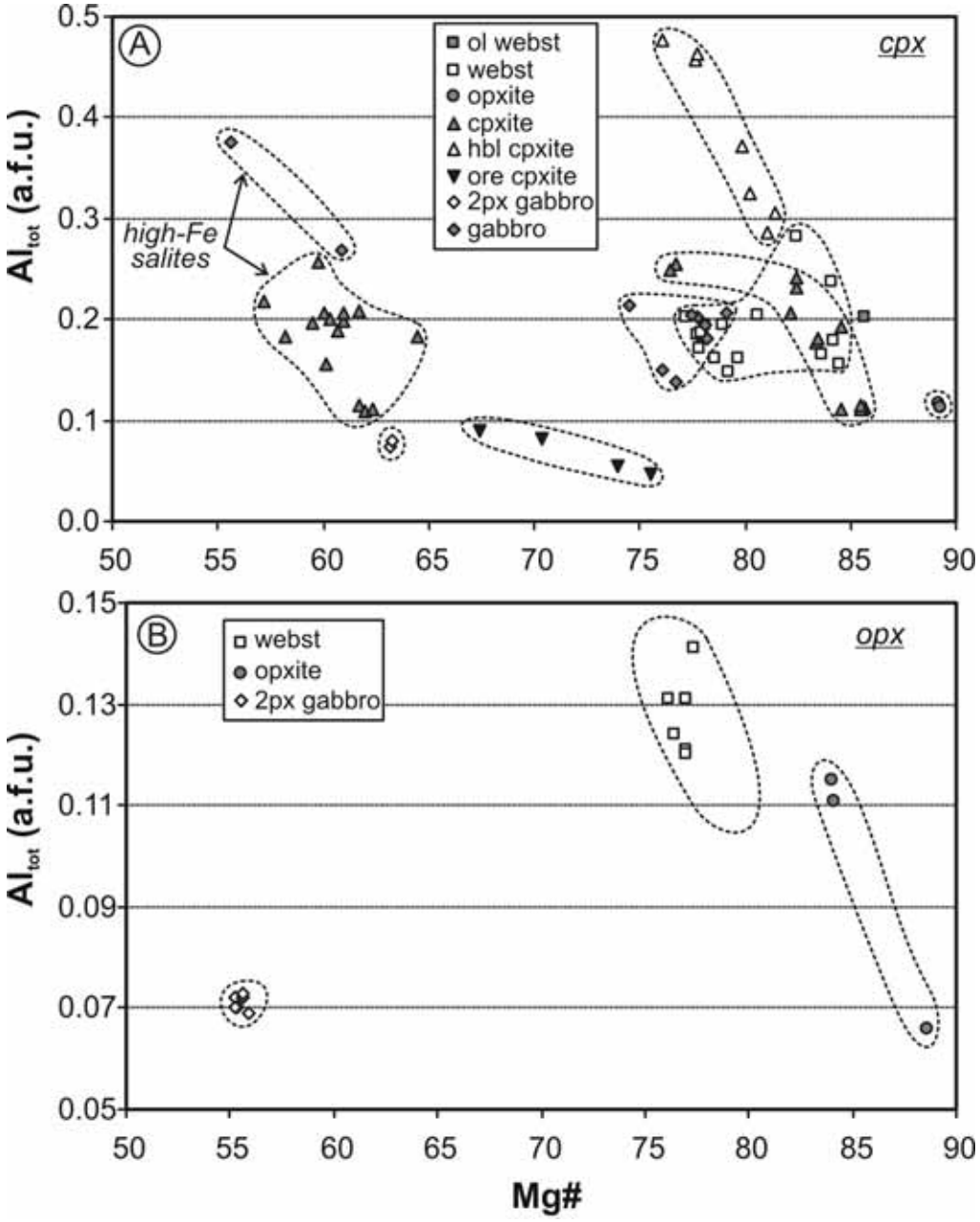

Figure 6. Correlation between Al (a.f.u.) and Mg # (100 Mg + Fe) of (A) clinopyroxenes and (B) orthopyroxenes from the Krumovgrad xenoliths.

coexisting olivine-clinopyroxene in sample Bz24-3 yields a temperature of ~1200 °C, considerably higher than that of the clinopyroxene-orthopyroxene pair (1074 °C). The Fe-Ti oxide pair in the clinopyroxenite layer of the composite clinopyroxenite-gabbro xenolith Bz03-2/6 yields the lowest temperature in the entire xenolith suite, 850 °C. The estimated fO_2 at this temperature (-13.89) is slightly above that of the Ni-NiO buffer.

Depth of Crystallization of the Xenoliths. The pyroxenes have variable Al^{VI}/Al^{IV} ratios (0.05–2.84; Table 3). Except for some high-Fe clinopyroxenes, which plot in the field of low-pressure phenocrysts of volcanic rocks, most of them fall in the granulite-clinopyroxenite field of Aoki and Shiba (1973), implying pressures close to those of the lowermost crust and possibly those in the uppermost mantle (Fig. 7). The geobarometer

TABLE 5. REPRESENTATIVE MICROPROBE ANALYSES OF PLAGIOCLASE IN THE KRUMOVGRAD XENOLITHS

Rock type	Cpxite	Cpxite	Cpxite	Cpxite	Gabbro	Gabbro	2-px gabbro	2-px gabbro	2-px gabbro
Sample no.	Bz03-2/6 Center	Bz03-2/6 Rim	Bz03-2/5 Center	Bz03-2/5 Rim	Bz24-5c Center	Bz24-5c Rim	Bz24-5b Center	Bz24-5b Interm. zone	Bz24-5b Rim
SiO_2	55.60	56.39	53.75	54.03	53.60	56.29	55.76	56.50	64.32
TiO_2	0.02	0.01	0.00	0.03	0.00	0.01	0.04	0.00	0.07
Al_2O_3	27.45	26.62	29.46	29.22	29.73	27.58	27.59	26.78	21.55
Cr_2O_3	0.01	0.00	0.00	0.00	0.01	0.05	0.00	0.00	0.05
FeO	0.33	0.45	0.21	0.63	0.14	0.18	0.13	0.14	0.35
MnO	0.02	0.00	0.00	0.03	0.01	0.00	0.00	0.01	0.00
MgO	0.01	0.00	0.03	0.03	0.03	0.00	0.01	0.00	0.00
CaO	10.07	9.10	12.35	11.64	11.81	9.73	9.61	8.35	2.71
Na_2O	5.39	5.87	4.66	4.74	4.59	5.71	5.59	4.90	7.97
K_2O	0.53	0.69	0.09	0.36	0.34	0.42	0.53	2.98	3.02
Total	99.40	99.12	100.55	100.70	100.25	99.95	99.25	99.65	100.03
An	49.2	44.3	59.1	56.4	57.6	47.3	47.2	40.2	13.1
Ab	47.7	51.7	40.4	41.5	40.5	50.3	49.7	42.7	69.6
Or	3.1	4.0	0.5	2.1	2.0	2.4	3.1	17.1	17.3
Si	2.521	2.562	2.421	2.433	2.419	2.534	2.520	2.567	2.864
Ti	0.001	0.000	0.000	0.001	0.000	0.000	0.012	0.000	0.002
Al	1.467	1.425	1.564	1.551	1.581	1.463	1.470	1.434	1.131
Fe	0.013	0.017	0.008	0.024	0.005	0.007	0.005	0.005	0.013
Mn	0.001	0.000	0.000	0.001	0.000	0.000	0.000	0.000	0.000
Mg	0.001	0.000	0.002	0.002	0.002	0.000	0.001	0.000	0.000
Ca	0.489	0.443	0.596	0.562	0.571	0.469	0.465	0.407	0.129
Na	0.474	0.517	0.407	0.414	0.402	0.498	0.490	0.432	0.688
K	0.031	0.040	0.005	0.021	0.020	0.024	0.031	0.173	0.172

of Nimis (1995), based on cation distribution between M1 and M2 sites in the clinopyroxene structure, provides further constraints on the pressure conditions at which the xenoliths were formed. The calculations made using the Cpxbar program of Nimis and Ulmer (1998) and Nimis (1999) for hydrous basalt quartz to nepheline-normative mafic trachybasalt, basanite, tephrite, and mildly alkaline hydrous melts (discussed later) gave a pressure range for all the investigated xenoliths of 14–9 kilobars, decreasing from the ultramafic to the plagioclase-bearing gabbroic rocks (Table 8). Comparable pressures (14.9–11.3 kilobars) have been estimated by Dobosi et al. (2003) for the megacrysts and pyroxenite xenoliths from the Lake Balaton pliocene alkali basalts of the Pannonian basin, Hungary. Lower pressures (9–4 kilobars) were obtained by Kovács et al. (2004) for the pyroxenites from the neighboring Nógrád-Gömör volcanic field. The data obtained point to a depth interval of ~45–30 km for the equilibration of the xenoliths. The present-day Moho below the area is estimated at ~35 km (Velev, 1996; Papazachos and Skordilis, 1998), suggesting that most of the ultramafic xenoliths were equilibrated close to or beneath the current crust-mantle boundary zone.

Water Content (Volatile Components). The high-pressure experimental work of Müntener et al. (2001) with primitive basalts and high-Mg andesites clearly demonstrated that olivine-free, predominantly pyroxenite ultramafic plutonic rocks crystallized from hydrous (>3% H_2O) magmas in high-pressure (12 kilobars) conditions. According to these authors, high H_2O content suppresses plagioclase crystallization (see also Gaetani et al., 1993) and leads to the crystallization of amphibole and garnet. They also concluded that in the absence of a major alumina phase, the alumina in the liquids correlates positively with the Al in pyroxene, experimentally explaining the observed trends of increasing Al with fractionation in the arc-related pyroxenes in Talkeetna and Kohistan. The rarity of olivine is due to the narrow crystallization temperature interval of olivine-bearing assemblages and/or to peritectic reactions of the type olivine + liquid = pyroxenes.

The rarity of olivine-bearing varieties and the pressure estimates and chemistry of the pyroxenes of the Krumovgrad xenoliths match very well the experiments of Müntener et al. (2001), suggesting crystallization from comparatively hydrous primitive magma with more than 3 wt% H_2O. Additional evidence for the high water content of the ultramafic magma stems from the presence of early high-Cr amphibole in the wehrlite Eg97-1 and the comparatively low temperature of crystallization of the rock (1025–1000 °C).

TABLE 6. REPRESENTATIVE MICROPROBE ANALYSES OF AMPHIBOLE IN THE KRUMOVGRAD XENOLITHS

Rock type	Webst	Webst	Cpxite	Hbl cpxite	Hbl cpxite	Hbl x cpxite	Hbl cpxite	Hbl cpxite	Hbl cpxite	Hbl cpxite
Sample no.	EG97-1	EG97-1	IIEg7	Bz24-5a	Bz24-5a	Bz26-2a Core	Bz26-2a Interm. zone	Bz26-2a Interm. zone	Bz26-2a Interm. zone	Bz26-2a Rim
SiO_2	42.06	42.61	42.15	40.01	39.78	37.91	38.20	39.22	38.83	38.98
TiO_2	0.87	0.85	2.68	2.96	3.56	4.33	4.88	5.85	4.63	5.49
Al_2O_3	14.07	13.55	14.59	14.84	15.36	15.29	15.10	12.38	14.68	13.74
Cr_2O_3	0.58	0.67	0.32	0.08	0.03	0.02	0.02	0.02	0.08	0.09
FeO	11.45	10.53	7.83	8.73	8.83	15.87	12.34	13.01	11.51	8.89
MnO	0.19	0.14	0.07	0.13	0.16	0.27	0.19	0.29	0.14	0.11
MgO	14.58	15.00	15.41	13.56	13.81	9.24	11.09	10.75	11.21	12.42
CaO	10.65	10.66	11.28	12.26	12.23	11.70	11.66	11.75	11.48	11.47
Na_2O	3.08	3.25	2.36	2.45	2.26	2.39	2.44	2.52	2.30	2.36
K_2O	0.61	0.52	1.45	0.98	1.07	1.56	1.61	1.33	1.54	1.44
NiO		0.04	0.03	0.02					0.01	0.04
BaO	0.04				0.01	0.15	0.13	0.20		
SrO	0.16				0.15	0.16	0.08	0.27		
F	0.00				0.08	0.28	0.32	0.35		
Cl	0.03				0.01	0.04	0.04	0.04		
SO_3	0.03				0.00	0.08	0.08	0.07		
Total	98.14	97.82	98.17	96.01	97.09	98.58	97.53	97.12	96.41	95.01
Mg #	69.4	71.7	77.8	73.5	73.6	50.9	61.6	59.6	63.4	71.3
Si	5.994	6.083	6.007	5.949	5.831	5.694	5.705	5.896	5.851	5.891
Al^{IV}	2.006	1.918	1.993	2.051	2.169	2.307	2.295	2.104	2.149	2.108
Al^{VI}	0.357	0.362	0.458	0.550	0.485	0.400	0.363	0.089	0.458	0.339
Fe^{3+}	1.146	1.042	0.564	0.032	0.147	0.000	0.000	0.000	0.000	0.000
Fe^{2+}	0.219	0.215	0.369	1.054	0.935	1.993	1.541	1.636	1.451	1.124
Mg	3.097	3.192	3.274	3.006	3.018	2.069	2.469	2.409	2.517	2.798
Ca	1.626	1.630	1.722	1.953	1.921	1.883	1.866	1.892	1.853	1.858
Na	0.851	0.900	0.652	0.706	0.642	0.696	0.707	0.734	0.671	0.692
K	0.111	0.095	0.264	0.186	0.200	0.299	0.307	0.255	0.296	0.277
Ti	0.093	0.091	0.287	0.331	0.392	0.489	0.548	0.661	0.525	0.624
Mn	0.023	0.017	0.008	0.016	0.020	0.034	0.024	0.037	0.018	0.014
Cl	0.007	0.000	0.000	0.009	0.002	0.010	0.010	0.010	0.000	0.000
F	0.000	0.000	0.000	0.002	0.037	0.133	0.151	0.166	0.000	0.000
Cr	0.065	0.076	0.036		0.003	0.002	0.002	0.002	0.010	0.010
Ni	0.000	0.005	0.003		0.000	0.000	0.000	0.000	0.001	0.004
Ba	0.002	0.000	0.000		0.001	0.009	0.008	0.012	0.000	0.000
Sr	0.013	0.000	0.000		0.013	0.014	0.007	0.024	0.000	0.000

DISCUSSION

Comparison to Arc Cumulate Rocks and Xenoliths from Arc Magmas and Intraplate Basalts

Xenoliths that form series of ultramafic to gabbroic types are common in many calc-alkaline magmas of active arcs (e.g., the Aleutian arc; Conrad and Kay, 1984) or intraplate basalts (e.g., those of the Penghu islands, south China Sea, Ho et al., 2000; the East Eifel volcanic field, Sachs and Hansteen, 2000; Lake Balaton and the Nógrád-Gömör volcanic field, Pannonian basin, Hungary, Dobosi et al., 2003, and Kovács et al., 2004; and eastern Serbia, Cvetcović et al., 2004). To our knowledge, the only xenolith localities in the areas of extension and core complex formation were reported by Wilshire (1990) from the southwestern Basin and Range Province (USA) and by Çakir et al. (1999) from the Menderes massif (southwestern Turkey). Recently Marchev et al. (2004b) demonstrated that the eastern Rhodopes and these two regions experienced similar magmatic evolution, which ended with the intrusion of alkaline basalt. Wilshire (1990) described variable peridotites, igneous textured pyroxenites, and mafic to intermediate gabbros. An association of cumulate lherzolites, pyroxenites, hornblendites, and gabbros was described by Çakir et al. (1999). According to these authors,

TABLE 7. REPRESENTATIVE MICROPROBE ANALYSES OF OXIDES IN THE KRUMOVGRAD XENOLITHS

Rock type	Cpxite	Cpxite	Cpxite	Opxite	Hbl cpxite
Sample no.	Bz03-2/6	Bz03-2/6	Bz24	Bz24-1	Bz24-5a
Mineral	Mt	Ilm	Mt	Chr	Pleonast
SiO_2	0.11	0.20	0.04	0.02	0.00
TiO_2	21.73	50.56	9.93	0.40	0.16
Al_2O_3	1.69	0.16	3.23	17.25	59.80
Cr_2O_3	0.25	0.10	0.08	42.28	0.57
FeO	68.22	44.98	79.89	25.98	20.17
MnO	1.02	0.94	0.89	0.00	0.18
MgO	2.40	3.36	1.80	12.02	15.53
NiO	0.02			0.30	0.04
Total	95.44	100.30	95.86	98.25	96.45

hornblendites were the product of early segregation of the host magma, whereas the remaining xenoliths were formed during earlier volcanism.

Surface exposures of ultramafic to mafic cumulate complexes hundreds of meters to kilometers thick are described from the Talkeetna area, Alaska (De Bari and Coleman, 1989; DeBari and Sleep, 1991; Kelemen et al., 2003) and the Kohistan terrane of northern Pakistan (Khan et al., 1993; Miller and Christensen, 1994; Burg et al., 1998; Ringuette et al., 1999), the Ivrea zone in northern Italy (Mehnert, 1975; Rivalenti et al., 1981, 1984; Quick et al., 1994), and Cabo Ortegal (Galicia, northwestern Spain; Girardeau et al., 1989). These complexes have been interpreted to be the remnants of magma chambers emplaced at the base of the crust, close to the upper mantle–lower crust transition.

Generalized sections of the exposed arc cumulates include thick pyroxenites bracketed between underlying mantle peridotites and overlying gabbroic rocks with a transitional zone between them often containing garnet-bearing gabbroic lithologies. Small-sized deposits of Cu-Ni-Fe sulfides with minor quantities of ilmenite and magnetite and platinum-group minerals are typical of the pyroxenite sections of the Ivrea and Kohistan cumulates (Garuti et al., 1986, 1990; Miller et al., 1991).

Xenoliths from the eastern Rhodope lavas cover most of the xenolith types found in the exposed sections of ultramafic to mafic cumulate complexes. The most striking differences between the Krumovgrad and arc xenolith or cumulate complexes are the absence of garnet-bearing varieties and the An-poor composition of the plagioclases in the gabbroic types. The absence of garnet-bearing varieties can be explained by the incomplete sampling and/or by the rarity of the garnet rocks that usually comprise comparatively thin layers in the exposed sections. Another explanation could be the crystallization of the magmas at *P-T* conditions above the stability field of garnet. Experimental data on the crystallization of tholeiitic to high-alumina magmas at high pressure (Green, 1969, 1982) demonstrate that garnet and clinopyroxene appear on the liquidus at pressures from 18 to 27 kilobars and temperatures between 1200 and 1450 °C, although Müntener et al. (2001) synthesized garnet at pressures as low as 12 kilobars and temperatures of 1070–1110 °C. Alternatively, a higher content of H_2O in the eastern Rhodope mafic magmas could suppress the crystallization of garnet, causing the crystallization of amphibole instead (Müntener et al., 2001).

With their low-anorthite plagioclase, Krumovgrad gabbros are more similar to those from mid-ocean-ridge and ocean-island gabbros and from tholeiitic layered intrusions (see Beard, 1986). This is rather surprising, because in a hydrous system like that at Krumovgrad we would expect An-rich plagioclase. The most likely explanation for the low-calcic composition of the Krumovgrad gabbros is the depletion of Ca in the residual melt as the result of the early crystallization of a large amount of highly calcic clinopyroxene. Another possible explanation is the more evolved composition of the melts from which the Krumovgrad gabbroic xenolits crystallized compared to the more mafic lithologies in Kohistan and Tonsina. For example, in the Kohistan and Tonsina sections the most calcic plagioclase ($An_{98–83}$) coexists with pyroxenes of Mg # 87–68 (Khan et al., 1993; DeBari and Coleman, 1989), whereas the less calcic plagioclase in the lower-pressure gabbros from Kohistan ($An_{64–40}$) and

TABLE 8. REPRESENTATIVE ANALYSES OF SULFIDES IN THE KRUMOVGRAD XENOLITHS

Rock type	Ol webst	Ol webst	Ore cpxite	Ore cpxite	Ore cpxite	Gabbro	Gabbro	2-px gabbro
Sample no.	Bz24-3	Bz24-3	Eg97-4a	Eg97-4a	Eg97-4a	Bz24-5c	Bz03-2/5	Bz24-5b
Mineral	Pyrrhotite	Pyrrhotite	Pyrrhotite	Pyrite	Chalcopyrite	Pyrrhotite	Cubanite	Pyrrhotite
S	38.51	37.87	37.63	50.52	36.38	38.44	34.04	37.32
Fe	58.23	55.99	58.80	44.13	31.52	58.53	38.89	58.12
Ni	1.02	1.07	0.29	0.53	0.05	0.58	2.09	0.56
Co	0.20	0.30	0.11	0.19	0.04	0.18	0.26	0.07
Cu	0.05	0.06	0.00	0.06	27.83	0.02	20.47	0.02
Zn	0.00	0.03	0.00	0.07	0.07	0.00	0.05	0.00
Total	98.01	95.31	96.84	95.51	95.89	97.74	95.80	96.08

TABLE 9. TEMPERATURE AND PRESSURE ESTIMATION AFTER NIMIS (1999) AND NIMIS AND ULMER (1998) FOR CUMULATE XENOLITHS FROM KRUMOVGRAD

Rock type	Ol webst	Webst	Webst	Cpxite	Opxite	2-px gabbro
Sample no.	Bz24-3	Eg97-1	IIEG99-2	Bz03-2/6	Bz24-1	24-5b
T (°C) 2-px; Wood & Banno (1973)	1074–1043	1025–1010	977–988		1069	903
T (°C) 2-px; Wells (1977)	1026–986	1039–995	959–973		977	976
T (°C) 2-px QUILF	990 ± 25	1002–954 ± 23	928 ± 69; 949 ± 26		980 ± 21	823 ± 27
T (°C) Ol-Cpx (Loucks, 1996)	1189–1204					
T (°C) Mt-Ilm QUILF				850		
Log fO_2 QUILF				–13.9		
P (kilobars) MA	9.8–13.6	11.1–12.4	10.8–14.4		8.4–13.1	9.3–12.7
P (kilobars) BH	11.7–14.6	11.6–12.9	11.8–14.7		7.3–11.6	

Tonsina ($An_{83–62}$) coexists with lower-Mg clinopyroxenes (Mg # 75–54). The range of plagioclase in the Krumovgrad gabbros ($An_{59–40}$), coexisting with clinopyroxene of Mg # 79–55, is similar to that of the lower-pressure Kohistan and Tonsina gabbros and seems to crystallize from more evolved composition. Such a conclusion is in accord with the experiments of Müntener et al. (2001), who showed that the crystallization of plagioclase-bearing rocks occurs after up to 50% of the primary, mantle-derived magma crystallizes as ultramafic cumulates.

The results of this comparison suggest that the transition between mantle and crust in the eastern Rhodope metamorphic core complexes is similar to that in mature intraocean and continental arcs. The fact that similar xenoliths were found in arc lavas and intraplate basalts, including those erupted in the core complexes, indicates that the processes of mafic magma underplating and formation of large masses of cumulates are similar in both environments.

Parental Magma Composition

Attempts to identify the parental magmas of the pyroxenites from exposed cumulate sections and xenoliths lead to controversial results. Tholeiitic basaltic magma was suggested for the pyroxenites and gabbros in Talkeetna (DeBari and Sleep, 1991; Kelemen et al., 2003) and the gabbro complex in the Val Malenco, eastern Alps (Hermann et al., 2001). For the xenoliths in Cima volcanic field, southwestern Basin and Range Province, and Penghu island, south China Sea, two different parent magmas were suggested, one of alkaline and another of tholeiitic

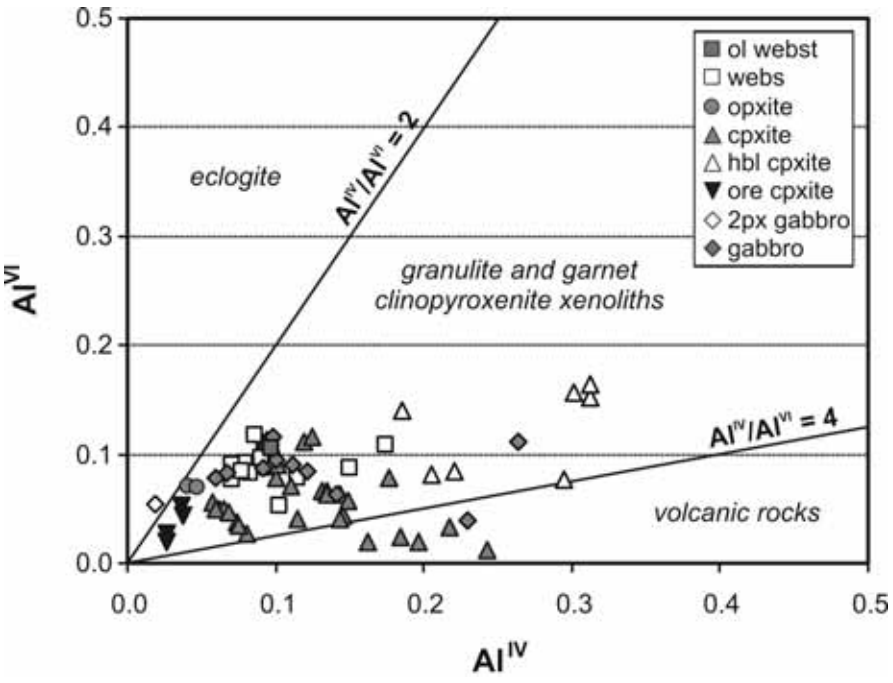

Figure 7. Compositions of the clinopyroxenes from the cumulate xenoliths of the Krumovgrad alkaline basalts in the Al^{IV}-Al^{VI} diagram. Fields from Aoki and Shiba (1973).

affinity. Alkaline parental magma was proposed for the xenoliths from the Pannonian basin, Hungary (Dobosi et al., 2003; Kovács et al., 2004).

The high Mg # of olivine, orthopyroxene, and clinopyroxene of most ultramafic xenoliths and bulk rock websterite from Krumovgrad and their high Ni and Cr contents are consistent with crystallization from a mafic mantle-derived magma. The amphibole and clinopyroxene in the amphibole clinopyroxenite Bz26-2a show a composition and zonation similar to those in megacrysts from the host lava. The amphibole is reversely zoned with iron-rich cores (Mg # 51), surrounded by more Mg-rich rims (Mg # 77–71). The clinopyroxene is enriched in TiO_2 and Al_2O_3 and depleted in SiO_2. These features are typical of the composition of phenocrysts in the host lamprophyres, suggesting that both megacrysts and amphibole clinopyroxenite Bz26-2a crystallized from closely related melts. The high-Na-Fe clinopyroxenes in the apatite-sulfide bearing clinopyroxenes and gabbros are analogous to those of the amphibole-apatite-bearing clinopyroxenites in southeastern China, which have been interpreted to precipitate from alkali-basalt magma at high pressure (Ho et al., 2000). High TiO_2 and Al_2O_3 concentrations and high Na_2O at a low Mg # are also typical of some clinopyroxenites and gabbros from the Canary islands, which are believed to have crystallized from alkaline melts (Neumann et al., 1999). Thus, it is inferred that at least some amphibole clinopyroxenites and high-Na-Fe salite clinopyroxenites and gabbros are geochemically linked to alkali-basalt magma.

Cumulate Bodies and Core Complex Formation

Estimation of the depth of crystallization by the method of Nimis (1999) and Nimis and Ulmer (1998) may yield a great deal of uncertainty, exceeding 4 kilobars. Nevertheless, the clustering of most geobarometry results for ultramafic xenoliths around 11–13 kilobars indicates that the base of the ultramafic part of the complex crystallized at depths near 35–40 km, whereas the more evolved two-pyroxene gabbros seem to have equilibrated at 30 km or less. Thus, these data provide evidence for the emplacement of the plutonic rocks within an interval of ~10–15 km, which is comparable with the sections of cumulate rocks exposed at the crust-mantle boundary of Kohistan (9 km, Miller and Christensen, 1994), Tolchina-Nelchina (~9 km, DeBari and Coleman, 1989; DeBari, 1997), and the Ivrea zone (5–15 km, Quick et al., 1994). The present-day Moho below the eastern Rhodope area is estimated at ~30–35 km (Velev, 1996; Papazachos and Skordilis, 1998), which appears to be ~5–10 km above the base of the equilibration depth of the deepest ultramafic xenoliths.

Uplift of the crust during intrusions of at least three successive intrusive events has been suggested by Rivalenti et al. (1984) to explain the large pressure range (10–6 kilobars) of the cumulate rocks from the Ivrea-Verbano basic complex compared to their smaller actual thickness (~2 km). The amount of uplift is similar to that (~10 km) proposed for the eastern Rhodopes by Krohe and Mposkos (2002), who suggested a thinning of the crust from 40 to 30 km as the result of Early Teriary extension and exhumation processes. On the other hand, Jull and Kelemen (2001) found that at appropriate conditions in arc settings or regions of crustal extension (e.g., T >1000 °C), a 10-km-thick ultramafic cumulate complex at the base of the crust would delaminate in less than one million years. Available data do not allow evaluation of the role of these two mechanisms in the eastern Rhodope area. However, what is obvious from the spectrum of entrained ultramafic to mafic xenoliths is that cumulate rocks still existed at the time of the extrusion of the intraplate basalts (28–26 Ma) and that if delamination of the lower crust occurred at all, it would have happened after this magmatic event.

Thermal and experimental modeling predicts that the magmatic underplating of large masses of hot magma at the base of the crust may significantly modify its thermal and mechanical properties, thus enhancing deformation and strain localization in an extensional environment (Furlog and Fountain, 1986; Gans, 1987; Wilshire, 1990; Fyfe, 1992; White, 1992; Corti et al., 2003). Ultramafic to mafic intrusions in the Ivrea zone can be regarded as important examples of such a process. Here, most regional studies have presumed that emplacement of the upper mafic complex provided the heat for regional granulite-facies metamorphism (Rivalenti et al., 1981; Sills, 1984; Sinigoi et al., 1996) and caused significant extension (Quick et al., 1994). The recent studies of Barboza and Bergantz (2000), however, demonstrated that the intrusion of the upper mafic complex postdates the prograde regional metamorphism, which the authors associated with the earlier lower mafic complex. Nevertheless, these authors admitted that although intrusion of the upper mafic complex did not cause the regional metamorphism, it provided enough thermal energy to reset mineral assemblages and induce anatexis within an aureole of ~3 km in the overlying supracrustal rocks.

The lack of precise timing of the ultramafic to mafic intrusion and the thermal events in the eastern Rhodope metamorphic core complexes precludes the provision of conclusive evidence for the role of the underplating mafic magma. An early prograde metamorphism of ca. 73.5 ± 3.4 Ma (Liati et al., 2002) is evident in the upper unit. The contemporaneity of this metamorphism with the intrusion of granitoids of ca. 70 Ma (Marchev et al., 2004b) can be interpreted in favor of a causal relationship between this magmatism and metamorphism. Although it is possible that the underplating of the mafic magma coincides with the Upper Cretaceous intrusion, the absence of deformation in the xenoliths suggests that they were formed later, most probably in the age interval of 40–31 Ma.

Figure 8 is a schematic illustration of our proposed model for the magmatism, thermal events, and Au deposits in the Krumovgrad area. Overprint and retrogression of the Late Cretaceous metamorphism by younger thermal events is indicated by abundant late Eocene (40–35 Ma) K-Ar (Lips et al., 2000; Krohe and Mposkos, 2002) and $^{40}Ar/^{39}Ar$ biotite and muscovite ages

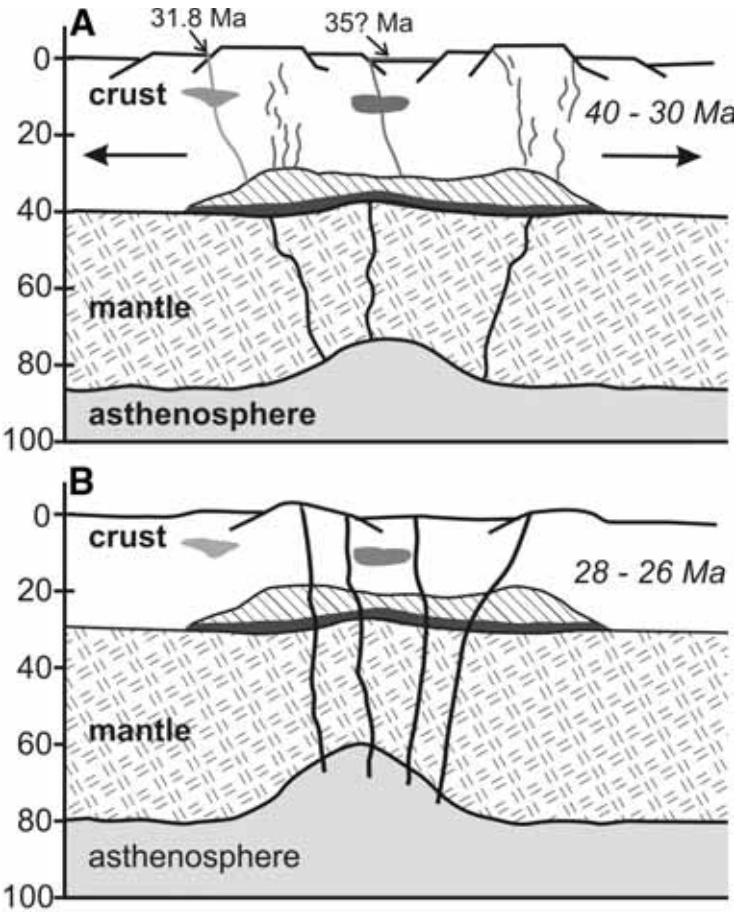

Figure 8. Schematic diagram illustrating metamorphic core complex formation with magmatic underplating and evolution of the magmatism in the eastern Rhodope massif. (A) Mafic magma(s) was emplaced at the crust-mantle boundary level, causing thermal reset and modification of mechanical properties and extension of the lower and middle crust. Fluid exsolution from the deep-seated magma produces Au deposits. Cumulate crystallization and stratification generates an ultramafic or gabbroic cumulate sequence and a new Moho at the top of the ultramafic sequence. (B) Continuing asthenospheric upwelling led to the formation of purely asthenospheric ocean island basalts and probably resulted in lowering of the older Moho boundary. Intrusion of these basalts disrupted upper-mantle spinel lherzolite and lower-crustal ultramafic or mafic cumulates, carrying them to the surface.

(Bonev et al., 2005), with temperatures reaching 300–350 °C, the blocking temperature of biotite and muscovite. This thermal effect may have been caused by the underplating of mafic magma at the crust-mantle boundary and lower-crustal levels. Intrusion of the mafic magma (Fig. 8A) would have caused modification of the thermal and mechanical properties and extension of the lower and middle crust. Underplated magma would have been cooled for several million years, producing a stratified ultramafic and gabbroic plutonic sequence. Gans and Bohrson (1998) proposed that in some rifts rapid extension of the crust may suppress volcanic activity, leading to widespread syn-extensional plutonism. Such rapidly extended rifts may be characterized by elevated heatflow and hydrothermal activity (see also Fyfe, 1992).

Early accumulation of magma at greater depths can also explain the older age of the Au mineralization at Ada tepe and the Rosino deposits with respect to the local volcanic activity (Marchev et al., 2004a). It is interesting to note that similar Au mineralization (e.g., at Picacho, Liebler, 1988; Riverside Pass, Wilkinson et al., 1988; Whipple-Buckskin-Rawhide, Spencer and Welty, 1986) has been established in the core complex structures of the southwestern Basin and Range. According to Sillitoe and Hedenquist (2003), if the exsolved fluids from the deep-seated mafic magmas ascended rapidly, they could have produced Au veins from silica and Au colloids, similar to those described by Saunders (1994) and Marchev et al. (2004a).

Late Oligocene intraplate magmatism subsequent to the late Eocene magmatism and thermal metamorphism indicates that there was further upwelling of the asthenosphere under the eastern Rhodopes and decompression melting of the mantle that produced ocean-island basalt–type magmas (Fig. 8B). This event does not seem to have resulted in prograde metamorphism, probably due to the fast transport of the magma from the asthenosphere to the surface.

CONCLUSIONS

Study of the xenoliths in the Krumovgrad alkaline basalts suggests that the Kessebir and Biala reka metamorphic core complexes are underlain by masses of ultramafic to mafic plutonic complex of olivine websterites, othopyroxenites, clinopyroxenites, websterites, and gabbros. The crystallization sequence and mineral composition of the xenoliths are typical of ultramafic to mafic sections exposed in island- and continental-arc cumulate complexes and of xenoliths in arc and intraplate lavas. The chemistry of mafic minerals is consistent

with derivation of the plutonic sequence from primitive hydrous magma(s).

The finding of xenocrystic clinopyroxenes similar to those in xenoliths in the rocks dated 31–32 Ma indicate that the age of intrusion of the ultramafic to mafic complex is considerably older than the host dikes (26–28 Ma). We suggest that the thermal event and late-stage crustal extension and exhumation at 40–37 Ma and the Au deposition at ~36–35 Ma were probably related to the intrusion of mafic magma(s) that produced the layered complex. The later intrusion of intraplate basalts indicates further upwelling of the asthenosphere under the eastern Rhodopes and decompression melting of the hot asthenospheric mantle.

The layered plutonic rocks under the Kesebir and Biala reka metamorphic core complexes are the best candidates for the roots of the magmatism intruded at the crust-mantle boundary. The underplating of mafic magma(s) seems to have been a fundamental process that caused extension, formation of the metamorphic core complexes, and hydrothermal activity in the eastern Rhodopes, the Basin and Range, and Menderes massif. A further assessment of this model requires additional seismic work in the eastern Rhodope region combined with age and isotopic studies of the xenoliths, local magmatism, and mineralization.

ACKNOWLEDGMENTS

This study was carried out cooperatively between the Bulgarian Academy of Sciences (Geological Institute) and the Consiglio Nazionale della Ricerche (University of Florence). Partial funding for this work was provided by the Japan Society for Promotion of Science. Special thanks go to Miki Shirasaka and Filippo Olmi for their help with microprobe analyses. We gratefully acknowledge Rick Conrey for his help in improving our English. Critical reviews by Peter Thy and James Beard significantly improved an early version of this article. We thank Yildirim Dilek and Spiros Pavlides for their efforts in organizing this volume.

REFERENCES CITED

Andersen, D.J., Lindsley, D.H., and Davidson, P.M., 1993, QUILF: A Pascal program to assess equilibria among Fe-Mg-Mn-Ti oxides, pyroxenes, olivine, and quartz: Computers & Geosciences, v. 19, p. 1333–1350, doi: 10.1016/0098-3004(93)90033-2.

Aoki, K., and Shiba, I., 1973, Pyroxenes from lherzolite inclusions of Itinomegata, Japan: Lithos, v. 6, p. 41–51, doi: 10.1016/0024-4937(73)90078-9.

Arculus, R.J., 1978, Mineralogy and petrology of Grenada, Lesser Antilles island arc: Contributions to Mineralogy and Petrology, v. 65, p. 413–424, doi: 10.1007/BF00372288.

Barboza, S.A., and Bergantz, G.W., 2000, Metamorphism and anatexis in the Mafic Complex Contact Aureole, Ivrea Zone, Northern Italy: Journal of Petrology, v. 41, p. 1307–1327, doi: 10.1093/petrology/41.8.1307.

Beard, J., 1986, Characteristic mineralogy of arc-related cumulate gabbros: Implications for tectonic setting of gabbroic plutons and for andesite genesis: Geology, v. 14, p. 848–851, doi: 10.1130/0091-7613(1986)14<848:CMOACG>2.0.CO;2.

Bence, A.E., and Albee, A.L., 1968, Empirical correction factors for the electron microanalysis of silicate and oxides: Journal of Geology, v. 76, p. 382–403.

Bonev, N., 2002, Structure and evolution of the Kesebir gneiss dome, Eastern Rodopes [Ph.D. thesis]: University of Sofia, Sofia, 282 p. (in Bulgarian).

Bonev, N., Marchev, P., and Singer, B., 2005, $^{40}Ar/^{39}Ar$ geochronology constraints on the Middle Tertiary basement extensional exhumation, and its relation to ore-forming and magmatic processes in the Eastern Rhodope (Bulgaria): Geodinamica Acta, in press.

Boyanov, I., and Goranov, A., 1994, Paleocene–Eocene sediments from the Northern periphery of the Borovica depression and their correlation with similar sediments in the East Rhodopean Paleogene depression: Review of the Bulgarian Geological Society, v. 55, p. 83–102.

Boyanov, I., and Goranov, A., 2001, Late Alpine (Paleogene) superimposed depressions in parts of Southeast Bulgaria: Geologica Balcanica, v. 34, p. 3–36.

Burg, J.P., Ivanov, Z., Ricou, L.E., Dimor, D., and Klain, L., 1990, Implications of shear-sense criteria for the tectonic evolution of the Central Rhodope Massif, Southern Bulgaria: Geology, v. 18, p. 451–454, doi: 10.1130/0091-7613(1990)018<0451:IOSSCF>2.3.CO;2.

Burg, J.-P., Ricou, L.-E., Ivanov, Z., Godfriaux, I., Dimov, D., and Klain, L., 1996, Syn-metamorphic nappe complex in the Rhodope Massif: Structure and kinematics: Terra Nova, v. 8, p. 6–15.

Burg, J.P., Bodinier, J.L., Chaudhry, S., Hussain, S., and Dawood, H., 1998, Infra-arc mantle-crust transition and intra-arc mantle diapirs in the Kohistan complex (Pakistani Himalaya): Petro-structural evidence: Terra Nova, v. 10, p. 74–80, doi: 10.1046/j.1365-3121.1998.00170.x.

Çakir, U., Aydar, E., Sen, E., and Bayhan, H., 1999, Petrographic characteristics of ultramafic-mafic nodules in alkali basalts from Kula Province, western Anatolia, Turkey: EUGIO Journal of Conference Abstracts, Cambridge Publications, v. 4.

Carrigan, C., Mukasa, S., Haydoutov, I., and Kolcheva, K., 2003, Ion microprobe U-Pb zircon ages of pre-Alpine rocks in the Balkan, Sredna Gora, and Rhodope terranes of Bulgaria: Constraints on Neoproterozoic and Variscan tectonic evolution: Journal of the Czech Geological Society, v. 48, p. 32–33.

Chèry, J., Daignières, M., Lucazeau, F., and Vilotte, J.-P., 1989, Strain localization in rift zones (case of thermally softened lithosphere): A finite element approach: Bulletin de la Société Géologique de France, v. 8, p. 437–443.

Conrad, W.K., and Kay, R.W., 1984, Ultramafic and mafic inclusions from Adak Island: Crystallization history and implications for the nature of primary magmas and crustal evolution in the Aleutian island arc: Journal of Petrology, v. 25, p. 88–125.

Corti, G., Bonini, M., Innocenti, F., Manetti, P., Conticelli, S., Innocenti, F., Manetti, P., and Sokutis, D., 2003, Analogue modeling of continental extension: A review focused on the relationships between patterns of deformation and the presence of magma: Earth Science Review, v. 63, p. 169–247, doi: 10.1016/S0012-8252(03)00035-7.

Coward, M.P., Windley, B.F., Broughton, R.D., Luff, I.W., Petterson, M.G., Pudsey, C.J., Rex, D.C., and Asif Khan, M., 1986, Collision tectonics in the NW Himalayas: Geological Society of London Special Publication 19, p. 203–219.

Cvetković, V., and Downes, H., Prelević, D., Jovanović, M., and Lazarov, M., 2004, Characteristics of the lithospheric mantle beneath East Serbia inferred from ultramafic xenoliths in Palaeogene basanites: Contributions to Mineralogy and Petrology, v. 148, p. 335–357.

DeBari, S.M., 1997, Evolution of magmas in continental and oceanic arcs: The role of the lower crust: Canadian Mineralogist, v. 35, p. 501–519.

DeBari, S.M., and Coleman, R.G., 1989, Examination of the deep levels of an island arc: Evidence from the Tonsina ultramafic-mafic assemblage, Tonsina, Alaska: Journal of Geophysical Research, v. 94, p. 4373–4391.

DeBari, S.M., and Sleep, N.H., 1991, High-Mg, low-Al bulk composition of the Talkeetna island arc, Alaska: Implications for primary magmas and the nature of arc crust: Geological Society of America Bulletin, v. 103, p. 37–47.

Dinter, D.A., and Royden, L., 1993, Late Cenozoic extension in northeastern

Greece: Strimon Valley detachment and Rhodope metamorphic core complex: Geology, v. 21, p. 45–48, doi: 10.1130/0091-7613(1993)021<0045:LCEING>2.3.CO;2.

Dobosi, G., Downes, H., Embey-Isztin, A., and Jenner, G.A., 2003, Origin of megacrysts and pyroxenite xenoliths from the Pliocene alkali basalts of the Pannonian Basin (Hungary): Neues Jahrbuch Abhandlungen, v. 178, no. 3, p. 217–237, doi: 10.1127/0077-7757/2003/0178-0217.

Furlog, K.P., and Fountain, D.M., 1986, Continental crustal underplating: Thermal consideration and seismic-petrologic consequences: Journal of Geophysical Research, v. 91, p. 8285–8294.

Fyfe, W.S., 1992, Magma underplating of continental crust: Journal of Volcanology and Geothermal Research, v. 50, p. 33–40, doi: 10.1016/0377-0273(92)90035-C.

Gaetani, G.A., Grove, T.L., and Bryan, W.B., 1993, The influence of water on the petrogenesis of subduction-related igneous rocks: Nature, v. 365, p. 332–334, doi: 10.1038/365332a0.

Gans, P.B., 1987, An open-system, two-layer crustal stretching model for the eastern Great Basin: Tectonics, v. 6, p. 1–12.

Gans, P.B., and Bohrson, W.A., 1998, Suppression of volcanism during rapid extension in the Basin and Range Province, United States: Science, v. 279, p. 66–68, doi: 10.1126/science.279.5347.66.

Gans, P.B., Mahood, G.A., and Schermer, E., 1989, Synextensional magmatism in the Basin and Range province: A case study from the Eastern Great Basin: Geological Society of America Special Paper 233, 53 p.

Garuti, G., Fiandri, P., and Rossi, A., 1986, Sulfide composition and phase relations in the Fe-Ni-Cu ore deposits of the Ivrea-Verbano basic complex (western Alps, Italy): Mineralium Depositita, v. 21, p. 22–34.

Garuti, G., Naldrett, A.J., and Ferrario, A., 1990, Platinum group elements in magmatic sulfides from the Ivrea Zone: Their control by sulfide assimilation and silicate fractionation: Economic Geology and the Bulletin of the Society of Economic Geologists, v. 85, p. 328–336.

Geoffroy, L., 1998, Diapirism and intraplate extension—Cause or consequence: Comptes Rendus de l'Académie des Sciences, Série II: Sciences de la Terre et des Planets, v. 326, p. 267–273, doi: 10.1016/S1251-8050(97)86817-6.

Girardeau, J., Gil Ibarguchi, J.I., and Ben Jamaa, N., 1989, Evidence for a heterogeneous upper mantle in the Cabo Ortegal complex, Spain: Science, v. 245, p. 1231–1233.

Goranov, A., and Atanasov, G., 1992, Lithostratigraphy and formation conditions of Mastrichtian-Paleocene deposit in Krumovgrad District: Geologica Balcanica, v. 22, p. 71–82.

Green, T.H., 1969, High pressure experimental studies on the origin of anorthosites: Canadian Journal of Earth Sciences, v. 6, p. 427–440.

Green, T.H., 1982, Anatexis of mafic crust and high pressure crystallization of andesite, *in* Thorpe, R.S., ed., Andesites: New York, John Wiley and Sons, p. 456–487.

Harkovska, A., Yanev, Y., and Marchev, P., 1989, General features of the Paleogene orogenic magmatism in Bulgaria: Geologica Balcanica, v. 19, p. 37–72.

Haydoutov, I., Kolcheva, K., Daieva, L., and Savov, I., 2001, Island-arc origin of the variegated formations from the East Rhodopes (Avren synform and Bela Reka antiform), Bulgaria. Abstacts, Joint Meeting of EUROPROBE TESZ, TIMPEBAR, URALIDES and SW–IBERIA projects, 30 September–2 October, Middle East Technical University, Ankara, Turkey, p. 31–32.

Hermann, J., Müntener, O., and Günter, D., 2001, Differentiation of mafic magma in a continental crust-to-mantle transition zone: Journal of Petrology, v. 42, p. 189–206, doi: 10.1093/petrology/42.1.189.

Hill, E.J., Baldwin, S.L., and Lister, G.S., 1995, Magmatism as an essential driving force for formation of active metamorphic core complexes in eastern Papua New Guinea: Journal of Geophysical Research, v. 100, p. 10,441–10,451, doi: 10.1029/94JB03329.

Ho, K.S., Chen, J.C., Alan, D.S., and Juang, W.S., 2000, Petrogenesis of two groups of pyroxenite from Tungchihsu, Penghu Islands, Taiwan Strait: Implications for mantle metasomatism beneath SE China: Chemical Geology, v. 167, p. 355–372, doi: 10.1016/S0009-2541(99)00237-5.

Ivanov, Z., 1989. Structure and tectonic evolution of the central parts of the Rhodope massif: Guide to excursion E3, XIV Congress of the Carpathian-Balkan Geological Association, 126 p.

Ivanov, Z., Dimov, D., and Sarov, S., 2000, Tectonic position, structure and tectonic evolution of the Rhodopes massif, *in* Ivanov, Z., ed., Structure, Alpine evolution and mineralizations of the Central Rhodope area (South Bulgaria): ABCD–GEODE 2000 workshop, Borovets, Sofia University, Sofia, Bulgaria, p. 1–20.

Jull, M., and Kelemen, P.B., 2001, On the conditions for lower crustal convective instability: Journal of Geophysical Research, v. 106, p. 6423–6446, doi: 10.1029/2000JB900357.

Kelemen, P.B., Hanghøj, K., and Greene, A.R., 2003, One view of the geochemistry of subduction-related magmatic arcs, with an emphasis on primitive andesite and lower crust, *in* R.L. Rudnick, ed., The crust, v. 3: Treatise on Geochemistry, ed. H.D. Holland and K.K. Turekian: Oxford, Elsevier-Pergamon, p. 593–659.

Khan, M.A., Jan, M.Q., and Weaver, B.L., 1993, Evolution of the lower arc crust in Kohistan, N. Pakistan: Temporal arc magmatism through early, mature and intra-arc rift stages: Geological Society of London Special Publication 74, p. 123–138.

Kovács, I., Zajacz, Z., and Szabó, C., 2004, Type-II xenoliths and related metasomatism from the Nógrád-Gömör Volcanic Field, Carpathian-Pannonian region (northern Hungary–southern Slovakia): Tectonophysics, v. 393, p. 139–161, doi: 10.1016/j.tecto.2004.07.032.

Kozhoukharov, D., Kozhoukharova, E., and Papanikolaou, D., 1988, Precambrian in the Rhodope massif, *in* Zoubek, V., ed., Precambrian in younger fold belts. Chichester, John Wiley and Sons, p. 723–778.

Krohe, A., and Mposkos, E., 2002, Multiple generations of extensional detachments in the Rhodope Mountains (northern Greece): Evidence of episodic exhumation of high-pressure rocks, *in* Blundell, D.J., et al., eds., The Timing and location of major ore deposits in an evolving Orogen: Geological Society of London Special Publication 204, p. 151–178.

Liati, A., and Gebauer, D., 1999, Constraining the prograde and retrograde P-T-t path of Eocene HP-rocks by SHRIMP dating of different zircon domains: Inferred rates of heating, burial, cooling and exhumation for central Rhodope, northern Greece: Contributions to Mineralogy and Petrology, v. 135, p. 340–354, doi: 10.1007/s004100050516.

Liati, A., and Gebauer, D., 2001, Palaeozoic as well as Mesozoic sedimentation and polymetamorphism in Central Rhodope (N. Greece) as inferred from U-Pb SRIMP-dating of detrital zircons: EUG XI Journal of Conference Abstracts, Cambridge Publications, v. 6, p. 315.

Liati, A., Gebauer, D., and Wysoczanski, R., 2002, U-Pb SHRIMP-dating of zircon domains from UHP garnet-rich mafic rocks and late pegmatoids in the Rhodope zone (N. Greece): Evidence for Early Cretaceous crystallization and Late Cretaceous metamorphism: Chemical Geology, v. 184, p. 281–299, doi: 10.1016/S0009-2541(01)00367-9.

Liebler, G.S., 1988, Geology and gold mineralization at the Picacho mine, Imperial County, California, *in* Schafer, R.W., et al., eds., Bulk mineable precious metal deposits of the Western United States: Symposium Proceedings, Geological Society of Nevada, Reno/Sparks, Nevada, Part IV: Gold-silver deposits associated with detachment faults, p. 453–504.

Lips, A.L.W., White, S.H., and Wijbrans, J.R., 2000, Middle–Late Alpine thermotectonic evolution of the southern Rhodope Massif, Greece: Geodinamica Acta, v. 13, p. 281–292, doi: 10.1016/S0985-3111(00)00042-5.

Lister, G.S., and Baldwin, S.L., 1993, Plutonism and the origin of metamorphic core complexes: Geology, v. 21, p. 607–610, doi: 10.1130/0091-7613(1993)021<0607:PATOOM>2.3.CO;2.

Loucks, R.R., 1996, A precise olivine-augite Mg-Fe-exchange geothermometer: Contributions to Mineralogy and Petrology, v. 125, p. 140–150, doi: 10.1007/s004100050211.

Lynch, H.D., and Morgan, P., 1987, The tensile strength of the lithosphere and the localisation of extension, *in* Coward et al., eds., Tectonics: Geological Society of London Special Publication 28, p. 53–65.

MacCready, T., Snoke, A.W., Wrigth, J.E., and Howard, K., 1997, Midcrustal

flow during Tertiary extension in the Ruby Mountains core complex, Nevada: Geological Society of America Bulletin, v. 109, p. 1576–1594, doi: 10.1130/0016-7606(1997)109<1576:MCFDTE>2.3.CO;2.

Marchev, P., Harkovska, A., Pecskay, Z., Vaselli, O., and Downes, H., 1997, Nature and age of the alkaline basaltic magmatism southeast of Krumovgrad, SE-Bulgaria: Comptes Rendus of the Bulgarian Academy of Sciences, v. 50, no. 4, p. 77–80.

Marchev, P., Rogers, G., Conrey, R., Quick, J., Vaselli, O., and Downes, H., 1998a, Paleogene orogenic and alkaline basic magmas in the Rhodope zone: Relationships, nature of magma sources, and role of crustal contamination: Acta Vulcanologica, v. 10, p. 217–232.

Marchev, P., Vaselli, O., Downes, H., Pinarelli, L., Ingram, G., Rogers, G., and Raicheva, R., 1998b, Petrology and geochemistry of alkaline basalts and lamprophyres: Implications for the chemical composition of the upper mantle beneath the Eastern Rhodopes (Bulgaria): Acta Vulcanologica, v. 10, p. 233–242.

Marchev, P., Singer, B., Andrew, C., Hasson, A., Moritz, R., and Bonev, N., 2003, Characteristics and preliminary $^{40}Ar/^{39}Ar$ and $^{87}Sr/^{86}Sr$ data of the Upper Eocene sedimentary-hosted low-sulfidation gold deposits Ada Tepe and Rosino, SE Bulgaria: Possible relation with core complex formation, *in* Eliopoulos, D., et al., eds., Mineral exploration and sustainable development: Rotterdam, Millpress, p. 1193–1196.

Marchev, P., Singer, B., Jelev, D., Hasson, S., Moritz, R., and Bonev, N., 2004a, The Ada Tepe deposit: A sediment-hosted and detachment fault-controlled low-sulfidation gold mineralization in the Eastern Rhodopes, SE Bulgaria: Swiss Bulletin of Mineralogy and Petrology, v. 84, p. 59–78.

Marchev, P., Raicheva, R., Downes, H., Vaselli, O., Chiaradia, M., and Moritz, R., 2004b, Compositional diversity of Eocene–Oligocene basaltic magmatism in the Eastern Rhodopes, SE Bulgaria: Implications for genesis and tectonic setting: Tectonophysics, v. 393, p. 301–328, doi: 10.1016/j.tecto.2004.07.045.

Mavroudchiev, B., 1964, Petrology of basaltic magmatism in the Krumovgrad area: Annuaire de l'Université de Sofia, Faculté de Géologie et Géographie, v. 57, p. 295–324.

Mehnert, K.R., 1975, The Ivrea zone. A model of the deep crust: Neues Jahrbuch für Mineralogie Abhandlungen, v. 125, p. 156–199.

Miller, D.J., and Christensen, N.I., 1994, Seismic signature and geochemistry of an island arc: A multidisciplinary study of the Kohistan accreted terrane, northern Pakistan: Journal of Geophysical Research, v. 99, p. 11,623–11,642, doi: 10.1029/94JB00059.

Miller, D.J., Loucks, R.R., and Ashraf, M., 1991, Platinum-group element mineralization in the Jijal layered ultramafic-mafic complex, Pakistani Himalayas: Economic Geology and the Bulletin of the Society of Economic Geologists, v. 86, p. 1093–1102.

Mposkos, E., and Krohe, A., 2000, Petrological and structural evolution of continental high pressure (HP) metamorphic rocks in the Alpine Rhodope Domain (N. Greece), *in* Panayides, I., et al., eds., Proceedings of the 3rd International Conference on the Geology of the Eastern Mediterranean (Nicosia, Cyprus): Nicosia, Cyprus, Geological Survey, p. 221–232.

Mposkos, E., and Wawrzenitz, N., 1995, Metapegmatites and pegmatites bracketing the time of high-P metamorphism in polymetamorphic rocks of the E-Rhodope, N. Greece: Petrological and geochronological constraints: Proceedings XV Congress of the Carpathian-Balkan Geological Association, Geological Society of Greece Special Publication 4, p. 602–608.

Mukasa, S., Haydoutov, I., Carrigan, C., and Kolcheva, K., 2003, Thermobarometry and $^{40}Ar/^{39}Ar$ ages of eclogitic and gneissic rocks in the Sredna Gora and Rhodope terranes of Bulgaria: Journal of the Czech Geological Society, Abstracts, v. 48, p. 94–95.

Müntener, O., Kelemen, P.B., and Grove, T.L., 2001, The role of H_2O during crystallization of primitive arc magmas under uppermost mantle conditions and genesis of igneous pyroxenites: An experimental study: Contribution to Mineralogy and Petrology, v. 141, p. 643–658.

Neumann, E.-R., Wulff-Pedersen, E., Simonsen, S.L., Pearson, N.J., Martí, J., and Mitjavila, J., 1999, Evidence for crustal crystallization of periodically refilled magma chambers in Tenerife, Canary Island: Journal of Petrology, v. 40, p. 1089–1123, doi: 10.1093/petrology/40.7.1089.

Nimis, P., 1995, A clinopyroxene geobarometer for basaltic systems based on crystal-structure modeling: Contributions to Mineralogy and Petrology, v. 121, p. 115–125, doi: 10.1007/s004100050093.

Nimis, P., 1999, Clinopyroxene geobarometry of magmatic rocks, Part 2: Structural geobarometers for basic to acid, tholeiitic and mildly alkaline magmatic systems: Contributions to Mineralogy and Petrology, v. 135, p. 62–74, doi: 10.1007/s004100050498.

Nimis, P., and Ulmer, P., 1998, Clinopyroxene geobarometry of magmatic rocks, Part 1: An expanded structural geobarometer for unhydrous and hydrous, basic and ultrabasic systems: Contributions to Mineralogy and Petrology, v. 133, p. 122–135, doi: 10.1007/s004100050442.

Ovtcharova, M., 2005, Petrology, geochronology and isotopic studies of metagranitoids from the eastern part of Madan-Davidkovo Dome [Ph.D. thesis]: University of Sofia, Sofia, 282 p. (in Bulgarian).

Ovtcharova, M.A., Cherneva, Z., von Quadt, A., and Peytcheva, I., 2002, Migmatic geochronology and geochemistry: A key to understanding the exhumation of the Madan dome (Bulgaria): Geochimica et Cosmochimica Acta, Abstracts of the 12th Annual Goldshmidt Conference, Davos, Switzerland, A573.

Papazachos, C.B., and Skordilis, E.M., 1998, Crustal structure of the Rhodope and surrounding area obtained by non-linear inversion of P and S travel times and its tectonic implications: Acta Vulcanologica, v. 10, p. 339–345.

Peytcheva, I., Kostitsin, Y., Salnikova, E., Kamenov, B., and Klain, L., 1998, Rb-Sr and U-Pb isotope data for the Rila-Rhodopes batholith: Mineralogy, Petrology and Geochemistry, v. 35, p. 93–105.

Peytcheva, I., von Quadt, A., Ovtcharova, M., Handler, R., Neubauer, F., Salnikova, E., Kostitsyn, Y., Sarov, S., and Kolcheva, K., 2004, Metagranitoids from the eastern part of the Central Rhodopean Dome (Bulgaria): U-Pb, Rb-Sr and $^{40}Ar/^{39}Ar$ timing of emplacement and exhumation and isotope-geochemical features: Mineralogy and Petrology, v. 82, p. 1–31, doi: 10.1007/s00710-004-0039-3.

Quick, J.E., Singoi, S., and Mayer, A., 1994, Emplacement dynamics of a large mafic intrusion in the lower crust, Ivrea-Verbano zone, northern Italy: Journal of Geophysical Research, v. 99, p. 21,559–21,573, doi: 10.1029/94JB00113.

Ricou, L.-E., Burg, J.-P., Godfriaux, I., and Ivanov, Z, 1998, Rhodope and Vardar: The metamorphic and olistostromic paired belts related to the Cretaceous subduction under Europe: Geodinamica Acta, v. 11, p. 285–309.

Ringuette, L., Martignole, J., and Winndley, B.F., 1999, Magmatic crystallization, isobaric cooling, and decompression of the garnet-bearing assemblages of the Jijal sequence (Kohistan terrane, western Himalayas): Geology, v. 27, p. 139–142, doi: 10.1130/0091-7613(1999)027<0139:MCICAD>2.3.CO;2.

Rivalenti, G., Garuti, G., Rossi, A., Siena, F., and Singoi, S., 1981, Existence of different peridotite types and of a layered igneous complex in the Ivrea Zone of the Western Alps: Journal of Petrology, v. 22, p. 127–153.

Rivalenti, G., Rossi, A., Siena, F., and Singoi, S., 1984, The layered series of the Ivrea-Verbano igneous complex, Western Alps, Italy: Tschermaks Mineralogische und Petrographische Mitteilungen, v. 33, p. 77–99, doi: 10.1007/BF01083065.

Sachs, P.M., and Hansteen, H.T., 2000, Pleistocene underplating and metasomatism of the lower continental crust: A xenolith study: Journal of Petrology, v. 41, p. 331–356, doi: 10.1093/petrology/41.3.331.

Saunders, J.A., 1994, Silica and gold texture in bonanza ores of the Sleeper deposit, Humbolt county, Nevada: Evidence for colloids and implications for epithermal ore-forming processes: Economic Geology and the Bulletin of the Society of Economic Geologists, v. 89, p. 628–638.

Sillitoe, R.H., and Hedenquist, J.W., 2003, Linkages between volcanotectonic settings, ore-fluid compositions, and epithermal precious metal deposits, *in* Simmons, S.F., and Graham, I., eds., Volcanic, geothermal, and ore-forming fluids: Rulers and witnesses of processes within the Earth: Society of Economic Geologists Special Publication 10, p. 315–343.

Sills, J.D., 1984, Granulite facies metamorphism in the Ivrea zone, N.W. Italy: Schweizerische Mineralogische und Petrographische Mitteilungen, v. 64, p. 169–191.

Sinigoi, S., Quick, J.E., Mayer, A., and Budahn, J., 1996, Influence of stretching and density contrast on the chemical evolution of continental magmas: An example from the Ivrea zone: Contributions to Mineralogy and Petrology, v. 123, p. 238–250, doi: 10.1007/s004100050153.

Spencer, J.E., and Welty, J.W., 1986, Possible controls of base- and precious-metal mineralization associated with Tertiary detachment faults in the lower Colorado River trough, Arizona and California: Geology, v. 14, p. 195–198, doi: 10.1130/0091-7613(1986)14<195:PCOBAP>2.0.CO;2.

Upton, B.G.J., Semet, M.P., and Joron, J.-L., 2000, Cumulate clasts in the Bellecombe Ash Member, Piton de la Fournaise, Reunion Island, and their bearing on cumulative processes in the petrogenesis of the Reunion lavas: Journal of Volcanology and Geothermal Research, v. 104, p. 297–318, doi: 10.1016/S0377-0273(00)00212-2.

Velev, A., 1996, Deep seismic reflection profiling of the Earth's crust along a regional profile Ivailovgrad-Ardino: Bulgarian Geophysical Journal, v. 22, p. 91–109.

Wells, P.R.A., 1977, Pyroxene thermometry in simple and complex systems: Contributions to Mineralogy and Petrology, v. 62, p. 129–139, doi: 10.1007/BF00372872.

White, R.S., 1992, Magmatism during and after continental break-up, *in* Storey, B.C., et al., eds., Magmatism and causes of continental break-up: Geological Society of London, Special Publication 68, p. 1–16.

Wilkinson, W.H., Wendt, C.J., and Dennis, M.D., 1988, Gold mineralization along Riverside Mountains Detachment Fault, Riverside County, California, *in* Schafer, R.W., et al., eds., Bulk mineable precious metal deposits of the Western United States: Symposium Proceedings, Geological Society of Nevada, Reno/Sparks, Nevada, Part IV: Gold-silver deposits associated with detachment faults, p. 487–504.

Wilshire, H.G., 1990, Lithology and evolution of the crust-mantle boundary region in the southwestern Basin and Range Province: Journal of Geophysical Research, v. 95, p. 649–665.

Wilson, M., and Downes, H., 1991, Tertiary–Quaternary extension-related alkaline magmatism in Western and Central Europe: Journal of Petrology, v. 32, p. 811–849.

Wood, B.J., and Banno, S., 1973, Garnet-orthopyroxene and orthopyroxene-clinopyroxene relationships in simple and complex systems: Contributions to Mineralogy and Petrology, v. 42, p. 109–124, doi: 10.1007/BF00371501.

Yanev, Y., and Bardintzeff, J.-M., 1997, Petrology, volcanology and metallogeny of Palaeogene collision-related volcanism of the Eastern Rhodopes (Bulgaria): Terra Nova, v. 9, p. 1–8, doi: 10.1046/j.1365-3121.1997.d01-3.x.

Yanev, Y., Innocenti, F., Manetti, P., and Serri, G., 1998, Upper-Eocene–Oligocene collision-related volcanism in Eastern Rhodopes (Bulgaria)–Western Thrace (Greece): Petrogenetic affinity and geodynamic significance: Acta Vulcanologica, v. 10, p. 279–291.

Zagortchev, I., and Moorbath, S., 1986, Problems of metamorphism in the Central Rhodope Mts in the light of Rb-Sr isotopic data: Geologica Balcanica, v. 16, p. 61–78.

Manuscript Accepted by the Society 30 December 2005

Printed in the USA